European Journal of Medicinal Chemistry 266 (2024) 116138

Contents lists available at ScienceDirect

European Journal of Medicinal Chemistry

journal homepage: www.elsevier.com/locate/ejmech

Research paper

Chromone-based small molecules for multistep shutdown of arachidonate pathway: Simultaneous inhibition of COX-2, 15-LOX and mPGES-1 enzymes

Perihan A. Elzahhar [a], Rebecca Orioli [b], Nayera W. Hassan [a], Silvia Gobbi [b], Federica Belluti [b], Hala F. Labib [c], Ahmed F. El-Yazbi [d,e], Rasha Nassra [f], Ahmed S.F. Belal [a,**], Alessandra Bisi [b,*]

[a] Department of Pharmaceutical Chemistry, Faculty of Pharmacy, Alexandria University, Alexandria, 21521, Egypt
[b] Department of Pharmacy and Biotechnology, Alma Mater Studiorum-University of Bologna, Via Belmeloro 6, 40126, Bologna, Italy
[c] Department of Pharmaceutical Chemistry, College of Pharmacy, Arab Academy of Science Technology and Maritime Transport, Alexandria, Egypt
[d] Faculty of Pharmacy and the Research and Innovation Hub, Alamein International University, Alamein, 5060335, Egypt
[e] Department of Pharmacology and Toxicology, Faculty of Pharmacy, Alexandria University, Alexandria, 21521, Egypt
[f] Department of Medical Biochemistry, Faculty of Medicine, Alexandria University, Egypt

ARTICLE INFO

Keywords:
Chromone
N-acylhydrazone
Inflammation
COX
15-LOX
mPGES-1

ABSTRACT

As a new approach to the management of inflammatory disorders, a series of chromone-based derivatives containing a (carbamate)hydrazone moiety was designed and synthesized. The compounds were assessed for their ability to inhibit COX-1/2, 15-LOX, and mPGES-1, as a combination that should effectively impede the arachidonate pathway. Results revealed that the benzylcarbazates (**2a-c**) demonstrated two-digit nanomolar COX-2 inhibitory activities with reasonable selectivity indices. They also showed appreciable 15-LOX inhibition, in comparison to quercetin. Further testing of these compounds for mPGES-1 inhibition displayed promising activities. Intriguingly, compounds **2a-c** were capable of suppressing edema in the formalin-induced rat paw edema assay. They exhibited an acceptable gastrointestinal safety profile regarding ulcerogenic liabilities in gross and histopathological examinations. Additionally, upon treatment with the test compounds, the expression of the anti-inflammatory cytokine IL-10 was elevated, whereas that of TNF-α, iNOS, IL-1β, and COX-2 were downregulated in LPS-challenged RAW264.7 macrophages. Docking experiments into the three enzymes showed interesting binding profiles and affinities, further substantiating their biological activities. Their *in silico* physicochemical and pharmacokinetic parameters were advantageous.

1. Introduction

Inflammation is a vital defence mechanism exerted by the body against external stimuli, resulting in physiological changes aimed at reducing tissue damage or combating pathogens [1]. If left uncontrolled, it can eventually cause chronic inflammatory ailments, autoimmune diseases, neurodegenerative disorders or even cancer [2]. The arachidonic acid (AA) signaling pathway, involving multiple enzymes and metabolites, is a trailblazer in the pathogenesis of inflammation [3]. Of particular interest, cyclooxygenase (COX), lipoxygenase (LOX), and microsomal prostaglandin E2 synthase 1 (mPGES1) are three metabolic enzymes that play a substantial role in AA metabolism and hence in mediating inflammation [4–6].

COXs (COX-1 and COX-2) catalyze the synthesis of prostaglandin H2 (PGH2), which is a precursor for the synthesis of various eicosanoids such as prostaglandins (PGs), prostacyclins (PGIs), and thromboxanes (TXs) [7,8]. Nonsteroidal anti-inflammatory drugs (NSAIDs) are the cornerstone of therapy of inflammation and act by inhibiting both COX-1 and COX-2 isoforms [9,10]. Despite their effectiveness, they are widely recognized to cause significant gastrointestinal problems because they effectively suppress the PGE2 produced *via* the COX-1 pathway [11]. Moreover, the discovery of coxibs as selective COX-2 inhibitors was thought to relieve the undesirable side effects associated with traditional NSAIDs, but the risk of myocardial infarction restricted their long-term use [12] Accordingly, the design of new COX-2 inhibitors with minimal side effects remains a major medicinal chemistry challenge.

Further, mPGES1 is a key enzyme in converting PGH2 to PGE2, which was found to be overexpressed in many inflammatory disorders [13] and human malignancies [14,15]; it is a glutathione

* Corresponding author.
** Corresponding author.
E-mail addresses: ahmed.belal@alexu.edu.eg (A.S.F. Belal), alessandra.bisi@unibo.it (A. Bisi).

https://doi.org/10.1016/j.ejmech.2024.116138
Received 7 November 2023; Received in revised form 8 January 2024; Accepted 9 January 2024
Available online 10 January 2024

Abbreviations

AA	arachidonic acid
COX	cyclooxygenase
LOX	lipoxygenase
mPGES1	microsomal prostaglandin E2 synthase 1
PGH2	prostaglandin H2
PGs	prostaglandins
PGIs	prostacyclins
TXs	thromboxanes
NSAIDs	nonsteroidal anti-inflammatory drugs
PUFAs	polyunsaturated fatty acids
NAH	N-acylhydrazone
ASA	acetylsalicylic acid
iNOS	inducible nitric oxide synthase
MOE	molecular operating environment
RMSD	root mean square deviation
LE	ligand efficiency
LLE	lipophilic ligand efficiency

(GSH)-dependent transmembrane enzyme that belongs to the MAPEG (membrane-associated proteins engaged in eicosanoid and glutathione metabolism) family [16]. Due to its direct impact on the production of PGE2, it has evolved as an outstanding target for developing safer anti-inflammatory drugs, lacking the classical NSAIDs side effects.

By shutting down the COX route, AA metabolism is diverted to the LOX pathway, through which polyunsaturated fatty acids (PUFAs), including AA, undergo stereo-specific peroxidation by lipoxygenases, producing the relative hydroperoxy derivatives [17,18]. Among LOX isozymes (5-, 12- and 15-LOX), the 15-LOX pathway produces lipoxins, which are pro-resolving and anti-inflammatory mediators [19]. On the other hand, the pro-inflammatory eoxins (also known as 14,15-leukotrienes) are also derived *via* the same pathway in eosinophils, mast cells, and nasal polyps from allergic subjects, indicating the controversial role played by the 15-LOX enzyme [17,20–22]. Considering this information, inhibition of 15-LOX could be a potential approach to diminish the biosynthesis of eoxins, hence treating several inflammatory conditions.

Therefore, simultaneously targeting COX-2, 15-LOX, and mPGES-1 enzymes would be an ideal strategy to develop new anti-inflammatory drugs with greater efficacy and safety. It should be noted that multi-target inhibitors of two out of these three targets (COX-2, 15-LOX and mPGES-1) have been described earlier [23,24], yet their triple inhibition has not been explored to our knowledge.

2. Design

Due to the well-known pivotal role played by COX enzymes in the development of inflammatory conditions, and considering that inhibition of COX-2 over COX-1 appears as a prominent requirement for treating inflammation without triggering the gastrointestinal side effects, a small series of easily affordable molecules were conceived as hybrids of properly selected pharmacophores, reported aCOX-2 isoform modulators.

In particular, the naturally-inspired chromone main scaffold was selected and decorated at positions 6 or 7 with a methoxy substituent, to evaluate the role of this group in activity. Indeed, a number of natural flavonoids bearing the chromone moiety (isorhamnetin, daidzein, and genistein, Fig. 1) have been recognized as inhibitors of LPS-induced COX-2 expression [25,26] and methoxychromones such as stellatin, the main constituent found in *Dysophylla stellata* (Labiatae), and its congener eugenin (Fig. 1) have also been described as selective COX-2 inhibitors endowed with anti-inflammatory properties [27]. Moreover, the novel synthetic small molecule iguratimod (IGU, Fig. 1) [28] is a disease-modifying anti-rheumatic drug routinely prescribed in Japan since 2012, and recently Rullah et al. reported the binding of a synthetic 7-methoxychromone derivative to COX-2 enzyme, postulating a possible role of this substituent in activity [29]. Likewise, among the natural products featuring the chromone scaffold as a basic structural element, quercetin showed promising 15-LOX inhibitory activity, while kaempferol and isorhamnetin (Fig. 1) proved to downregulate mPGES-1 expression in activated macrophages [30,31]. Taken together, these data allowed a wide validation of the prominence of the chromone structure in treating inflammatory-related conditions, and highlighted this *O*-heterocycle as a convenient framework to be properly functionalised in our hybridisation strategy.

In recent years, the *N*-acylhydrazone (NAH) fragment, which is considered a privileged structure in medicinal chemistry [32], has emerged as a key pharmacophore for COX inhibition, albeit its possible mechanism of action is still under debate [33]. A significant feature of

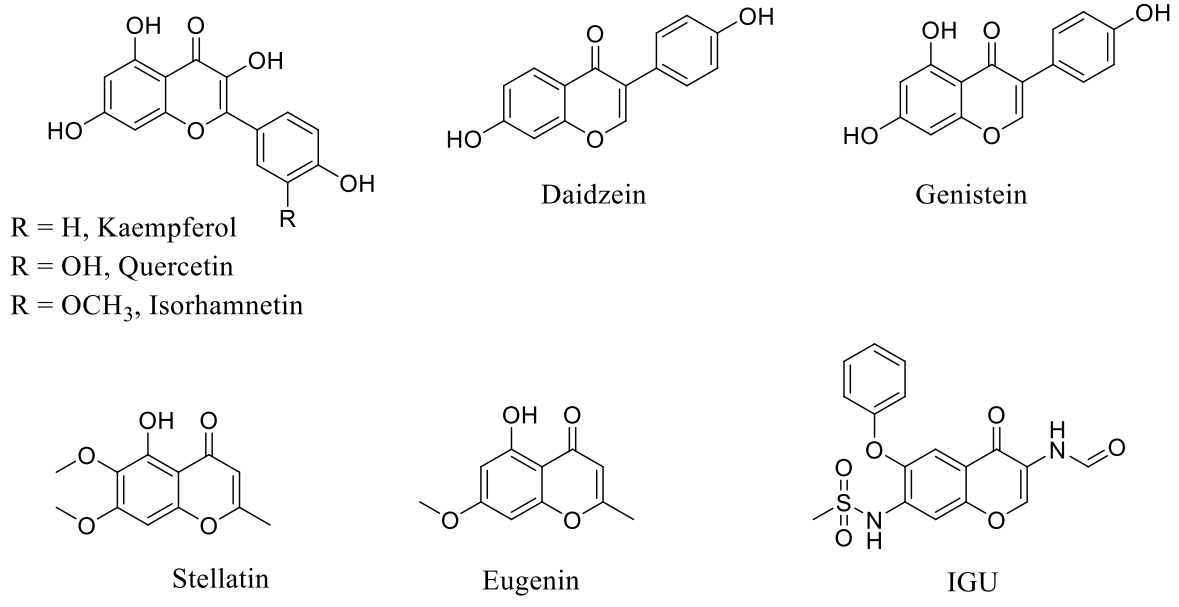

Fig. 1. Representative chromone-based inhibitors of COX-2 and mPGES-1 expression and/or activity or 15-LOX activity.

NAH-containing compounds lies in their recognized antiplatelet and antithrombotic activities, which may represent a valid premise for cardioprotective effects. Several studies have evaluated the impact of introducing this group into NSAIDs, and the hybridization of the NAH fragment with acetylsalicylic acid (ASA) (Structure A, Fig. 2) or different NSAIDs has been explored, leading to promising COX-inhibitors [34,35]. Interestingly, Noha et al. identified an *N*-acylhydrazone derivative (Structure B, Fig. 2) as an inhibitor of mPGES-1 (experimental IC_{50} of 4.5 μM) *via* a virtual screening protocol [36], validating the multipotent profile of this fragment.

A small library of hybrid compounds (**1a-c** and **2a-c**, Fig. 2 and Table 1) was thus designed by merging the (methoxy)chromone core and a NAH moiety in order to obtain triple COX-2, 15-LOX and mPGES-1 inhibitors. Aiming at modulating the reactivity of the NAH moiety, this portion was fused with a carbamate group, giving rise to a carbamate-hydrazone function, thus providing an additional oxygen atom with respect to NAH. This modification could grant a different hydrogen-bonding profile and a fine-tuned electrophilicity of the carbonyl group. Similar structures have been recently evaluated as potential chemical probes due to their peculiar reactivity profile, but their complete biological activities still deserve further in-depth studies [37]. To evaluate the role of the carbamate/acyl moiety on the hydrazone function, the corresponding methylhydrazone derivatives (**3a-c**, Table 1) were also synthesized.

Notably, the applied synthetic processess, albeit conventional, have been appropriately selected in a sustainability perspective, limiting the use of hazardous reagents to minimal amounts when possible. To this aim, some green chemistry practices have successfully been pursued, namely using minimal amounts of solvents, fast reaction times at moderately high temperatures, and very low waste production.

The designed compounds were evaluated for their abilities to modulate the activity of COXs, 15-LOX, and mPGES-1 enzymes. *In vivo* anti-inflammatory activity was then assessed for the most active compounds, and their effects on the expression levels of some inflammatory mediators were also evaluated.

3. Results and discussion

3.1. Chemistry

According to Scheme 1, compounds **1b-c**, **2a-c** and **3a-c** were prepared by refluxing the commercially available methylhydrazine, methylcarbazate or benzylcarbazate with the appropriately substituted aldehyde (4-oxo-4*H*-chromene-3-carbaldehyde, 6-methoxy-4-oxo-4*H*-chromene-3-carbaldehyde or 7-methoxy-4-oxo-4*H*-chromene-3-carbaldehyde) in ethanol. The compounds crystallized from the reaction mixture and were then further purified by recrystallization from ethanol. Compound **1a,** already reported in literature [38], was prepared by applying the same synthetic procedure. The aldehydes were obtained *via* a Vilsmeier-Haack formylation [39], by reacting the appropriate 2-hydroxyacetophenone with *N,N*-dimethylformamide and $POCl_3$, except for the commercially available 4-oxo-4H-chromene-3-carbaldehyde **4a** (formylchromone). The synthetized compounds were collected in Table 1.

Table 1
Structures of the synthesized compounds.

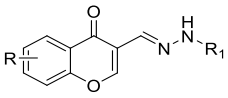

comp	R	R_1
1a [38]	H	$COOCH_3$
1b	6-OCH_3	$COOCH_3$
1c	7-OCH_3	$COOCH_3$
2a	H	$COOCH_2C_6H_5$
2b	6-OCH_3	$COOCH_2C_6H_5$
2c	7-OCH_3	$COOCH_2C_6H_5$
3a	H	CH_3
3b	6-OCH_3	CH_3
3c	7-OCH_3	CH_3

It is well-known that NAH bearing-compounds may exist as geometrical isomers (*E/Z*) with respect to the C=N double bond and as syn/antiperiplanar conformers due to the rotation of the NH–CO amide bond and its pseudo double bond character (Fig. 3) [40]. Looking at the ^{1}H NMR spectra of our compounds, only one set of signals was detected, suggesting that only one of the possible isomeric forms is present in DMSO-d_6 solution. According to literature data [41], this may be attributed to the formation of the less sterically hindered (*E*)-diastereomers. However, to better elucidate the stereochemistry, compound **1c** was selected to be further investigated by 1D-NOESY analysis by selective irradiation of the H-1 (CH=N $\delta = 8.15$ ppm) hydrogen. An interaction was observed with H-2 (N–NH, $\delta = 11.09$ ppm), consistent with the *E* isomer formation. Moreover, 2D-NOESY was also performed and the observed interactions between H-1 and H-2 confirmed the *E*-stereochemistry of the compound (see Supplementary Material). Regarding the NH–CO amide bond, the synthesized compounds feature this function as part of a carbamate moiety, and despite the close

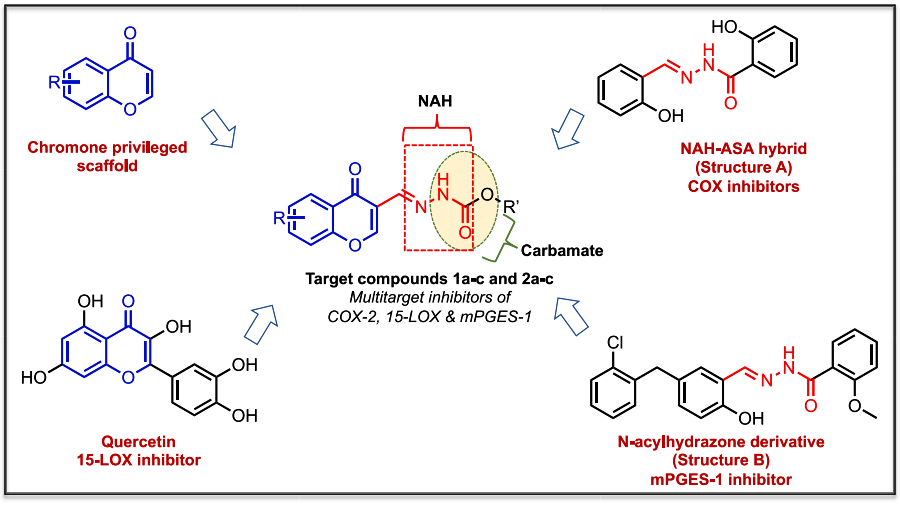

Fig. 2. Design of the new compounds.

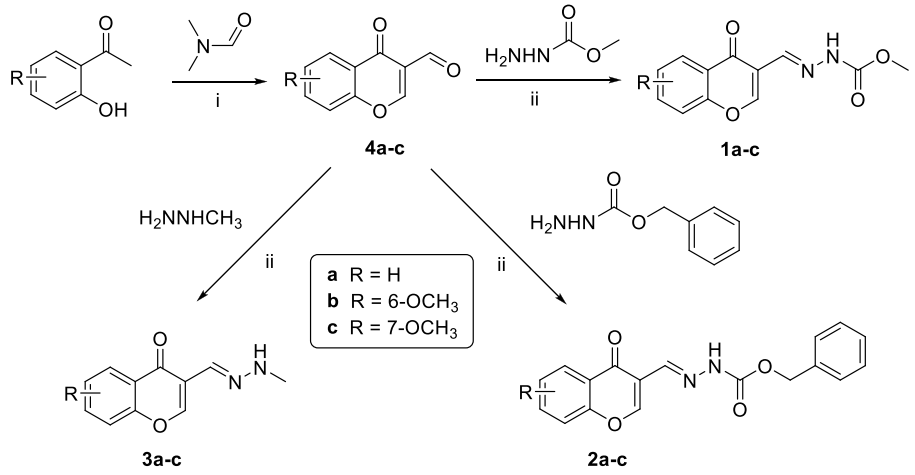

Scheme 1. Preparation of derivatives **1a-c**, **2a-c** and **3a-c**. Reagents and conditions: i) $POCl_3$, 60 °C, 2 h and rt overnight, c.y. 55–64 %; ii) ethanol, reflux, 1 h, c.y. 40–97 %.

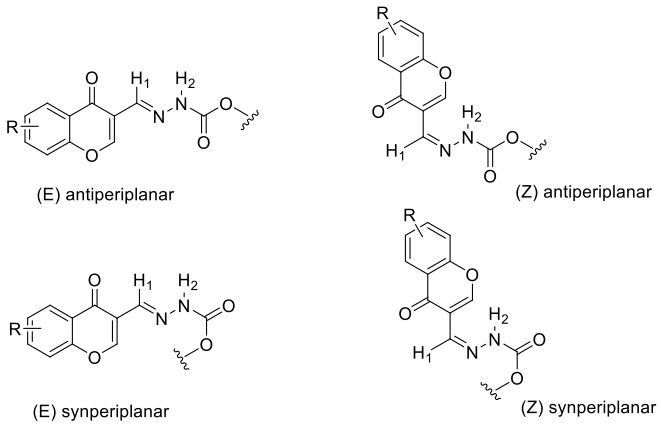

Fig. 3. Possible stereoisomers of the new compounds.

similarity to amides, several literature data [42,43] showed a preference for the anti-conformation.

3.2. Biological evaluation

3.2.1. In vitro COX-1 and COX-2 inhibitory activity

The synthesized compounds were tested to evaluate their *in vitro* COX-1/COX-2 inhibitory activities utilizing an ovine COX-1/human recombinant COX-2 assay kit. Concentrations suppressing 50 % of enzymatic activity (IC_{50}) were used to express the inhibitory activities of the tested compounds. Selectivity index (SI) values were also computed as IC_{50} (COX-1)/IC_{50} (COX-2). Indomethacin and diclofenac, representing non-selective COX inhibitors, as well as the selective COX-2 inhibitor celecoxib, were used as positive controls for comparison.

From the results reported in Table 2, it could be observed that all compounds showed improved COX-2 inhibitory activity with respect to diclofenac, and that they were also more selective COX-2 inhibitors than both diclofenac and indomethacin. In particular, five out of the nine synthesized compounds showed two-digit nanomolar IC_{50} values comparable to that of celecoxib, while the IC_{50} values of the other four compounds were in the submicromolar range. A deeper look into the results revealed that the benzylcarbazates (**2a-c**) showed higher inhibitory activity towards COX-2 than both methylcarbazates (**1a-c**) and *N*2-methylhydrazone derivatives (**3a-c**). Considering the substituents on the chromone scaffold, the unsubstituted benzylcarbazate **2a** showed nanomolar potency (IC_{50} value of 49 nM) and a SI of 250, placing it in the forefront in this study in terms of both activity and selectivity, with potency comparable to celecoxib (IC_{50} value 45 nM). A slight drop in activity occurred with the introduction of a 7-methoxy substituent (IC_{50} = 57 nM for **2c**), which was further decreased by shifting the methoxy group from 7- to 6-position (IC_{50} = 89 nM for **2b**). Notably, although SI values appeared generally lower when compared to the selective COX-2 inhibitor celecoxib, this aspect could be envisaged as an asset, leading to a reduction in cardiovascular thrombotic events, frequently encountered with highly selective COX-2 agents [44].

As for methylcarbazates, the unsubstituted chromone derivative **1a** exhibited almost half the activity of celecoxib (IC_{50} of 91 *vs* 45 nM). Potency was considerably reduced to 20 % and 13 % the activity of

Table 2
In vitro COX-1, COX-2, 15-LOX and mPGES-1 inhibitory IC_{50} values and COX SI values of studied compounds.

Code	IC_{50} μM[a] ± SD				SI COX-1/COX-2[b]
	COX-1	COX-2	15-LOX	mPGES-1	
1a	7.43 ± 0.1	0.091 ± 0.0	2.77 ± 0.1	3.70 ± 0.1	82
1b	6.92 ± 0.1	0.23 ± 0.01	4.08 ± 0.09	–	30
1c	6.01 ± 0.1	0.34 ± 0.01	4.59 ± 0.04	–	18
2a	12.23 ± 0.1	0.049 ± 0.0	1.72 ± 0.03	4.10 ± 0.1	250
2b	9.82 ± 0.1	0.089 ± 0.0	3.05 ± 0.1	4.90 ± 0.2	110
2c	11.12 ± 0.1	0.057 ± 0.01	2.39 ± 0.03	2.80 ± 0.1	195
3a	4.04 ± 0.1	0.19 ± 0.0	4.44 ± 0.1	–	82
3b	8.67 ± 0.03	0.093 ± 0.0	3.25 ± 0.03	–	94
3c	3.62 ± 0.1	0.473 ± 0.01	4.31 ± 0.02	–	8
Celecoxib	14.7 ± 0.2	0.045 ± 0.0	–	20.10 ± 0.1	327
Indomethacin	0.1 ± 0.01	0.080 ± 0.0	–	–	1.25
Diclofenac sodium	3.8 ± 0.03	0.84 ± 0.01	–	–	4.52
Quercetin	–	–	3.34 ± 0.1	–	–

[a] IC_{50} is the concentration (μM) required to produce 50 % inhibition of enzymatic activity. All values are expressed as mean of three replicates.
[b] Selectivity index (SI) = IC_{50} (COX-1)/IC_{50} (COX-2).

celecoxib upon introduction of the methoxy substituent at 6- and 7-positions, respectively (**1b** and **1c**).

With regard to *N*2-methylhydrazones, a different trend could be observed: the unsubstituted chromone derivative **3a** (IC_{50} = 190 nM) displayed 24 % the activity of celecoxib, which was greatly enhanced and almost doubled upon introduction of the 6-methoxy substituent (**3b**, IC_{50} = 93 nM). However, activity sharply decreased upon moving the substituent from the 6- to the 7-position (**3c**, IC_{50} = 470 nM).

3.2.2. *In vitro 15-LOX inhibitory activity*

The compounds were then tested to evaluate their *in vitro* lipoxygenase inhibition using Lipoxygenase inhibitor screening assay kit. The selective 12/15-LOX inhibitor quercetin was used as a reference for comparison. Generally speaking, all compounds showed single-digit micromolar IC_{50}s, which correspond to moderate to good 15-LOX inhibitory activity, and operated within the same order of magnitude as quercetin. The benzylcarbazate series appeared the most effective also on this enzyme, and the unsubstituted chromone derivative **2a** was the most potent 15-LOX inhibitor in this study (IC_{50} = 1.72 μM), showing almost double activity with respect to quercetin (IC_{50} 3.34 μM). **2b** and **2c** also proved to have potencies similar to quercetin, with 1.4 and 1.1 folds the reference's activity for **2c** and **2b**, respectively. Among the methylcarbazates, only the unsubstituted chromone derivative **1a** demonstrated significant 15-LOX inhibition, being 1.2 times more active than quercetin. The introduction of a methoxy group on the chromone core at 6- or 7-position (compounds **1b** and **1c)** lowered the activity to 80 % and 73 % that of quercetin, respectively. On the other hand, *N*2-methylhydrazone series followed a different pattern from the carbazates since the 6-methoxychromone derivative **3b** (IC_{50} = 3.25 μM) was found to be nearly equipotent to quercetin. Lower activities were recorded for the 7-methoxychromone and unsubstituted derivatives **3c** and **3a** (IC_{50}s = 4.31 and 4.44 μM, respectively).

3.2.3. *In vitro mPGES-1 inhibitory assay*

In order to span the outcome of this study on different stages of arachidonate-based inflammatory pathways, the most active compounds on both COX-2 and 15-LOX **2a-c** and **1a** were selected to be evaluated for mPGES-1 inhibitory activity. It is noteworthy to mention that mPGES-1 occurs downstream of COX and is responsible for converting PGH2 to the potent inflammatory PGE2 [45]. The protocol used for this assay is similar to well-established previously reported ones with some adaptations [46,47]. Celecoxib was again used as a positive control and showed an IC_{50} value quite similar to the reported one [45].

Intriguingly, all tested compounds showed good to moderate single-digit micromolar activity against mPGES-1 and were at least one order of magnitude more active than celecoxib. The benzylcarbazate chromone **2c** appeared the most active, with an IC_{50} of 2.8 μM. The other derivatives showed IC_{50} values in the 3.3–4.9 μM range, with the following descending order of potency: **1a** > **2a** > **2b**. Interestingly, kaempferol and isorhamnetin, which share a common chromone scaffold with our compounds, were reported to downregulate mPGES-1 expression in activated macrophages [31]. Yet, to the best of our knowledge, the compounds presented in this study are the first chromone-based mPGES-1 direct inhibitors. As such, they are the first simultaneous triple inhibitors of arachidonate pathway targets COX-2, 15-LOX and mPGES-1.

3.2.4. *In vivo anti-inflammatory activity assay*

The formalin-induced rat paw edema assay was used as a model of acute inflammation [24] to establish the *in vivo* anti-inflammatory efficacy of the most active compounds in the previous enzymatic inhibitory assays. Inflammation was induced by injecting formalin subcutaneously. The test compounds (**2a-c**) were given orally at a dosage of 5 mg/kg body weight. The inhibition of edema formation compared to the vehicle control was assessed after 4 h to determine the potency of the compounds with respect to the control [24]. As positive controls, celecoxib and diclofenac sodium were used. As shown in Fig. 4A, compounds **2a-c** were as effective as celecoxib and diclofenac in reducing rat paw edema volume.

3.2.5. *Gastric ulcerogenic activity and histopathological studies*

At this point, it seemed necessary to examine the possible ulcerogenic effects of compounds **2a-c** *in vivo*. Gross examination of the gastric mucosa of the isolated rat stomachs showed it to be normal with no ulcers after treatment with the test compounds, celecoxib and diclofenac (Fig. 5). Histopathological examination was performed to verify the presence of an inflammatory response in the stomach layers of the treated rats (Fig. 6). As predicted, celecoxib did not cause ulceration, resulting in an optimal gastrointestinal safety status. In addition, **2b** and **2c**-treated groups presented normal epithelium with a modest amount of inflammation characterized by increased submucosal inflammatory cells as well as slight dilation of submucosal blood vessels. Considering **2a** and diclofenac, normal epithelium, congested vessels, and abundant submucosal infiltration were detected.

3.2.6. *Effect on expression of inflammatory mediators*

Several studies have shown that 15-LOX activity is correlated to cytokine production in a variety of cell lines [24,48]. Specifically, 15-LOX and its metabolites have been demonstrated to trigger the production of an array of pro-inflammatory cytokines in macrophages, including interleukins (IL)-1β, 6, 12, and 15 [49]. As well, it has been indicated that COX-2 contributes to the production of IL-1β [24]. On the other hand, inducible nitric oxide synthase (iNOS), a crucial enzyme that controls inflammatory reactions, has been reported to be co-induced or co-regulated with COX-2 in many cell culture studies and animal models of inflammation [50].

In view of the above, we investigated the effects of the most active compounds **2a-c** on the expression levels of some inflammatory mediators in LPS-challenged RAW264.7 macrophages. As shown in Fig. 4B–F, 72-h incubation with a non-cytotoxic concentration of the selected compounds (50 μg/ml) downregulated the expression levels of TNF-α, iNOS, IL-1β and COX-2, resulting in 32–71 %, 32–95 %, 54–94 % and 33–93 % of the reduction produced by the reference celecoxib, respectively. Besides, the anti-inflammatory cytokine IL-10 was upregulated upon exposure to the test compounds, affording fold changes ranging from 43 % to 106 %, compared to celecoxib.

3.3. *Docking studies*

In order to elucidate the structural features responsible for the experimentally measured IC_{50}s for the investigated compounds, a docking study was performed for the most promising compounds **2a** and **2c** on COX-2, 15-LOX and mPGES-1 enzymes (For docking of compound **2c**, refer to Supplementary Material, Figs. S21–S23). This allowed us to rationalize the inhibitors' binding mode to the enzymes and to pinpoint their key interactions with the molecular targets. This was performed using Molecular operating environment software (MOE 2019.0102). The utilized MOE search algorithm and scoring function aided in the identification of the best binding docking poses. Moreover, binding energy scores, binding interactions with the nearby amino acid residues and orientation of the docked compounds relative to the co-crystalized ligand were used to investigate the binding affinities of the docked compounds towards the enzymatic active site.

3.3.1. *Docking into COX-2 active site*

Docking was performed into the active site of COX-2 enzyme (https://www.rcsb.org/structure/1CX2). In this regard, we validated our docking protocol by re-docking of the cocrystallized ligand yielding a retrieved pose with root mean square deviation (RMSD) of 0.38 Å and docking score of −9.3 kcal/mol.

Investigation of the binding profile of compound **2a** into COX-2 active site (Fig. 7) showcased a number of hydrogen bonding

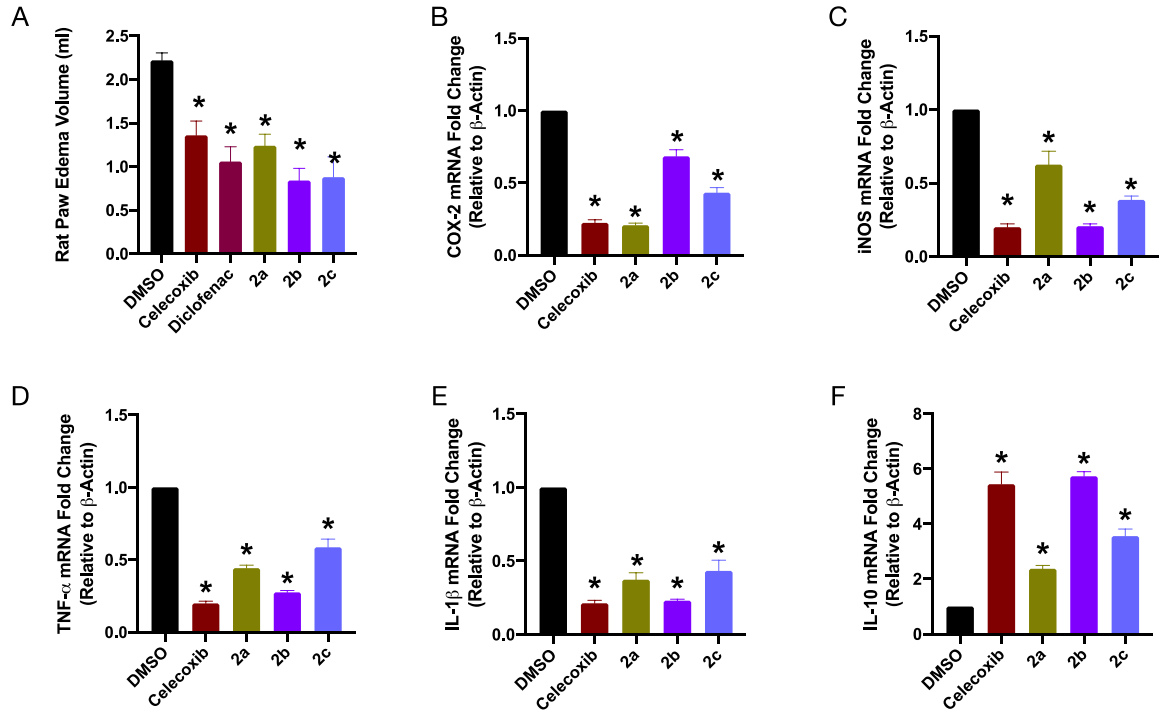

Fig. 4. ***In vivo*** **and** ***in vitro*** **anti-inflammatory activity of the selected test compounds in comparison to the reference COX inhibitor(s). (A)** Graphical representation of *in vivo* anti-inflammatory activities of the most active compounds **2a-c** in formalin-induced rat paw edema bioassay. **(B–F)** Graphical representation of fold changes in mRNA levels of different inflammatory mediators produced upon treatment of LPS-challenged RAW264.7 macrophages with compounds **2a-c**. Results presented are mean ± standard error of the mean of five separate experiments for (A) and three separate experiments for (B–F) replicates. Statistical analysis was performed using One-way ANOVA followed by Tukey post hoc test. A P-value <0.05 was considered significant. * denotes significance vs. DMSO.

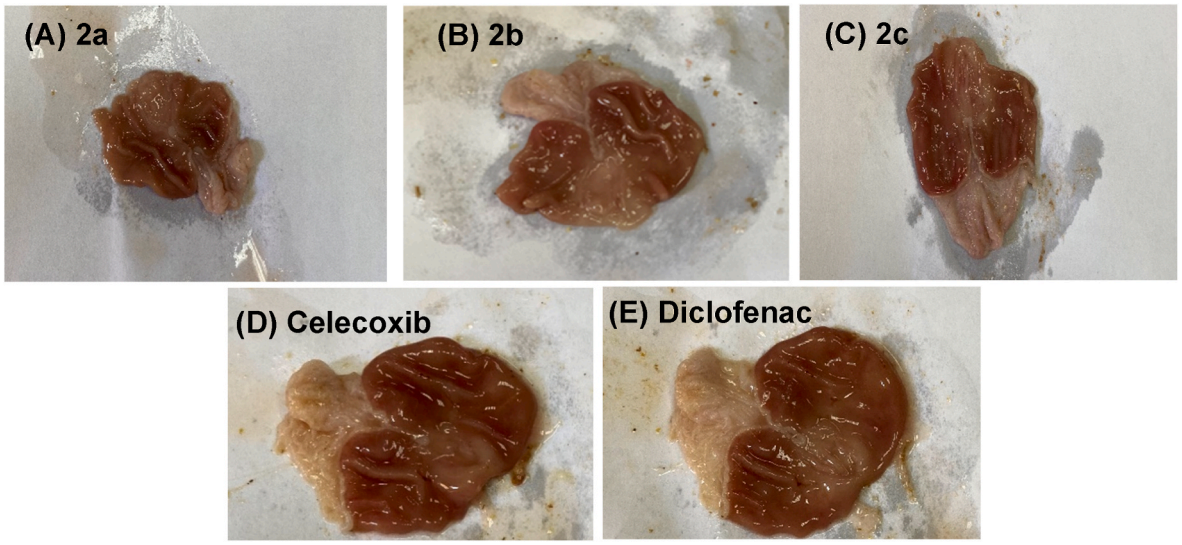

Fig. 5. Gross observation of the isolated rat stomachs.

interactions; two of which were formed between the imine nitrogen, as acceptor, and Val523 and Phe518 residues. Another two hydrogen bonds were displayed between NH, as donor, and the crucial amino acids His90 and Ser353. This is in addition to a hydrogen bond between the carbonyl oxygen of the carbazate group and Ala516. Various hydrophobic contacts were observed with His90, Thr94, Val349 and Gly354 (−7.4 kcal/mol).

3.3.2. *Docking into 15-LOX active site*

For the purpose of docking into the active site of 15-LOX enzyme (https://www.rcsb.org/structure/1LOX), pose-retrieval experiment was satisfactorily performed showing a root mean square deviation (RMSD) of 0.44 Å and docking score of −10.29 kcal/mol.

Docking experiments into 15-LOX pocket revealed that compound **2a** formed two hydrogen bonds, through carbonyl oxygen of the chromone ring, with Gln548 and Leu597 residues (Fig. 8). Another hydrogen bond was seen between carbonyl oxygen of the carbazate functionality and Ile400. In addition, three arene-hydrogen contacts with Leu408, Gln548 and Leu597 amino acids were spotted, and hence aiding in fortifying interactions (−7.9 kcal/mol).

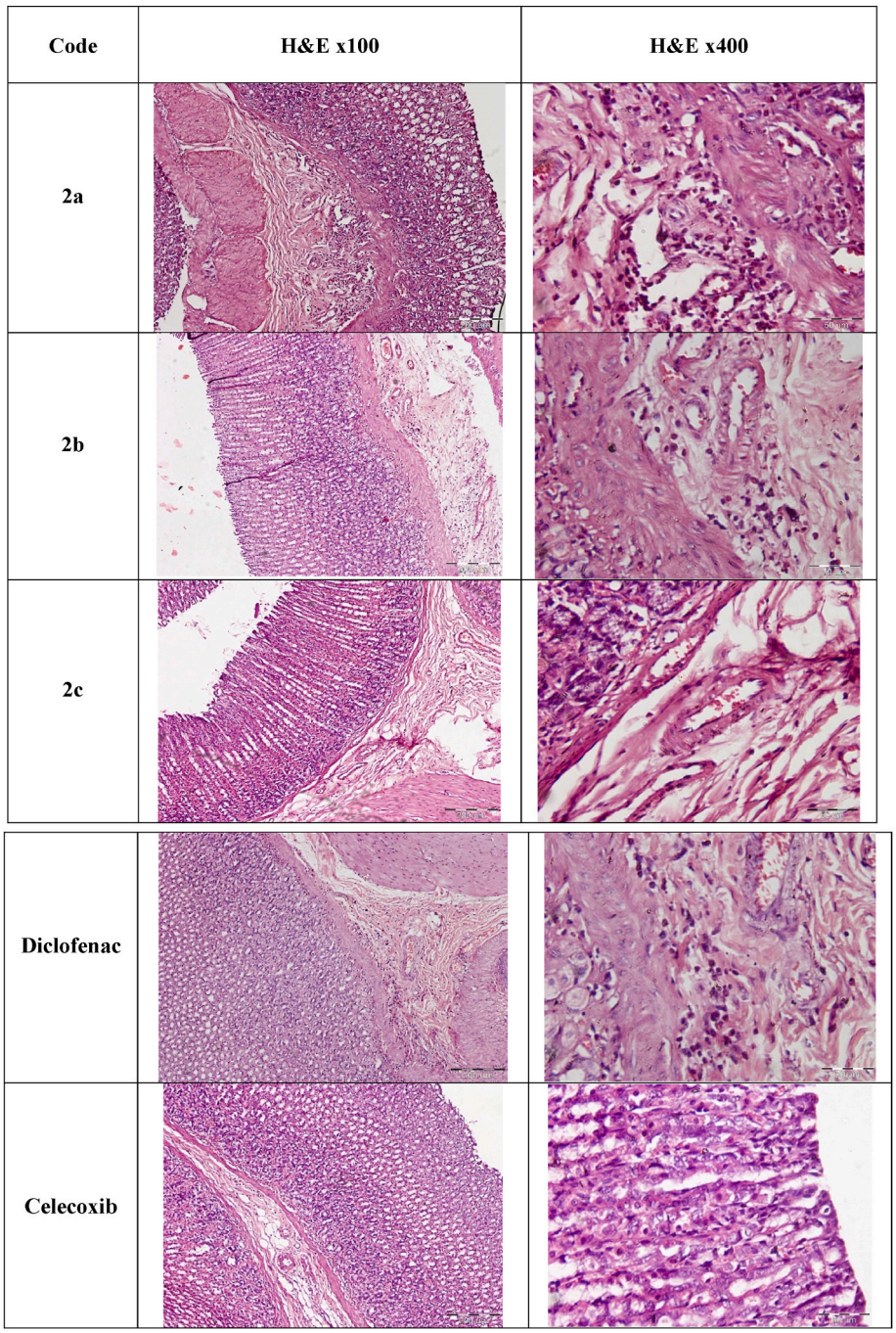

Fig. 6. Histopathological examination of stomach sections, treated with the test and reference compounds and stained with H&E.

3.3.3. *Docking into mPGES-1 active site*

A docking study was also carried out to characterize the possible molecular interactions involved in mPGES-1 recognition. The X-ray crystal structure of human mPGES1 (PDB ID: **4AL1**) with its co-crystallized ligand **48T** was obtained from protein data bank. (https://www.rcsb.org/structure/4al1). Re-docking of the co-crystallized ligand was also performed to validate the adopted docking protocol. The original pose generated from PDB was retrieved with root mean square deviation (RMSD) of 1.2 Å and a docking score of −5.4 kcal/mol.

Examination of the top-scored pose of compound **2a** (Fig. 9) revealed proper positioning within the active site *via* three hydrogen bonds: two of them between the acceptor carbonyl oxygen of the chromone ring and His113 and the essential residue Arg126. The latter interaction seems to be of an ultimate importance to the hindrance of the catalytic process. Another hydrogen bond was observed within the cofactor binding site, between the carbonyl oxygen of the ester group and Ser127. Extra binding interaction was also observed to the binding groove by two arene-hydrogen contacts between benzyl group and Tyr130 and Gln134 (−4.9 kcal/mol).

3.3.4. *In silico prediction of pharmacokinetic profile, drug likeness and ligand efficiency parameters*

In silico ADMET, drug likeness and ligand efficiency metrics were predicted for the two most active compounds **2a** and **2c** using molinspiration (http://www.molinspiration.com/cgi-bin/properties), Pre-ADMET (http://preadmet.bmdrc.org/adme-prediction/), ProTox-II (http://tox.charite.de/protox_II/) [51], SwissADME (http://www.swissadme.ch/) [52] and datawarrior (http://www.openmolecules.org/dat

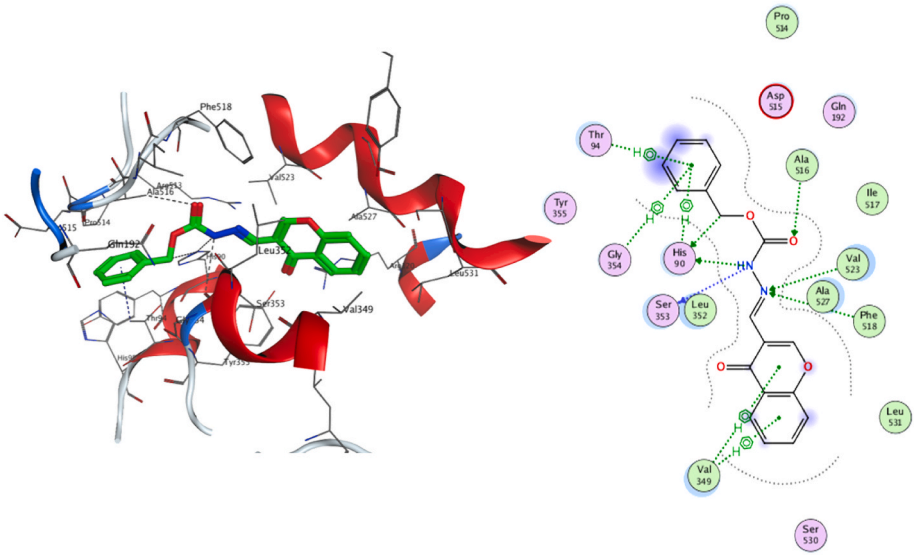

Fig. 7. Docking and binding pattern of compound **2a** into COX-2 active site (PDB 1CX2) in 3D (left panel), 2D (right panel) views.

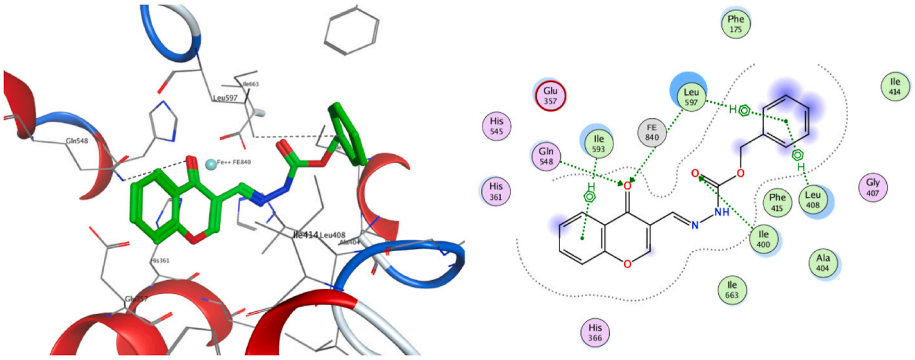

Fig. 8. Docking and binding pattern of compound **2a** into 15-LOX active site (PDB 1LOX) in 3D (left panel), 2D (right panel) views.

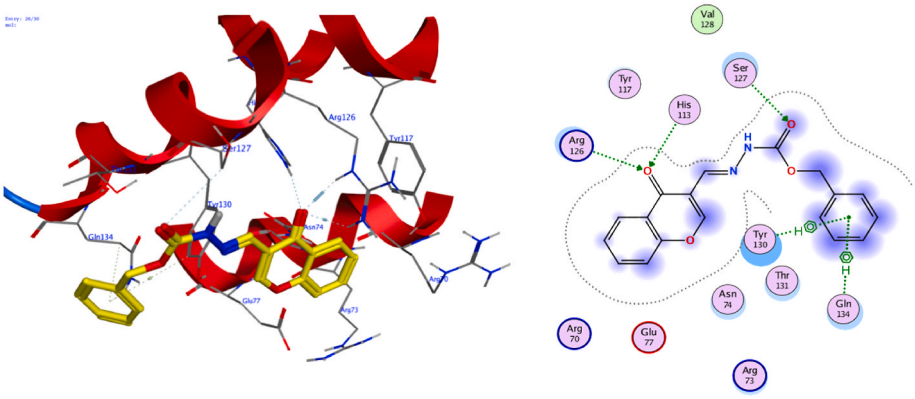

Fig. 9. Docking and binding pattern of compound **2a** into mPGES1active site (PDB 4AL1) in 3D (left panel), 2D (right panel) views.

awarrior/).

Results shown in Table 3 revealed that the test compounds did not violate Lipinski's rule parameters as they possessed good physicochemical properties (LogP, MW, number of hydrogen bond acceptors and donors). Topological polar surface area values were less than or equal to 90 A^2 (which is the accepted cutoff for CNS penetrating drugs), and the numbers of rotatable bonds were in the range of 4–6, as reported by Veber et al. [53].

Regarding pharmacokinetic profile, the compounds exhibited low to medium blood-brain barrier (BBB) penetration capability and were suggested to be poorly bound to plasma proteins. In addition, they displayed a high percentage of human intestinal absorption. The toxicity of the compounds was assessed using Pro Tox-II and proposed LD_{50} values from 400 to 2500 mg/kg.

SwissADME evaluates the drug-likeness of molecules relying on five commonly used rules (Lipinski, Muegge, Egan, Veber and Ghose). All tested compounds complied with these rules. Besides, the compounds were predicted to show no pan-assay interference potential (PAINS).

Table 3
In silico physicochemical properties, drug likeness and ligand efficiency parameters of compounds **2a** and **2c**.

	2a	2c
LogP[a]	3.32	3.35
MW[b]	322.32	352.35
HBA[c]	6	7
HBD[d]	1	1
TPSA[e]	80.91	90.14
Volume (A)^3	280.43	305.97
NROTB[f]	5	6
BBB[g]	0.1	0.03
HIA%[h]	96.4	96.8
Plasma protein binding[i]	84.2	86.2
Predicted LD50[j]	1002 mg/kg	2500 mg/kg
Lipinski's violation	0	0
Ghose violation	0	0
Veber violation	0	0
Egan #violations	0	0
Muegge #violations	0	0
PAINS #alerts[k]	0	0
LE[l] **(COX-2)**	0.42	0.38
LLE[m]	4.8	4.8
LE (15-LOX)	0.33	0.3
LLE	3.3	3.2
LE (mPGES)	0.3	0.29
LLE	2.9	3.1

[a] **LogP:** logarithm of compound partition coefficient between n-octanol and water.
[b] **MW:** molecular weight.
[c] **HBA:** number of hydrogen bond acceptors.
[d] **HBD:** number of hydrogen bond donors.
[e] **TPSA:** topological polar surface area.
[f] **NROTB:** number of rotatable bonds.
[g] **BBB:** blood-brain barrier penetration; BBB values < 0.1 (low CNS absorption), values from 0.1 to 2 (medium CNS absorption) and values > 2 (high CNS absorption).
[h] **HIA%:** percentage of human intestinal absorption; well absorbed compounds (70–100 %).
[i] **PPB:** plasma protein binding; PPB values < 90 % (poorly bound) and values > 90 % (strongly bound).
[j] **LD50:** Median lethal dose, Class IV: harmful if swallowed ($300 < LD50 \leq 2000$) and Class V: may be harmful if swallowed ($2000 < LD50 \leq 5000$).
[k] **PAINS #alerts**: pan assay interference alerts.
[l] **LE:** ligand efficiency.
[m] **LLE:** lipophilic ligand efficiency.

Furthermore, ligand efficiency (LE) indices were calculated for the three studied targets and collectively were in the range of 0.29–0.47, which conformed to accepted values for either leads (in the range of 0.3) or drug molecules (higher than 0.3) [54,55]. As well, lipophilic ligand efficiency (LLE) values were computed to be in the range of 2.9–6.8 and therefore satisfied the cutoff standards for leads (more than or equal to 3) or drugs (more than or equal to 5) [55–57].

4. Conclusions

In this paper, a small series of easily affordable chromone-NAH hybrids was reported, designed to counteract inflammation by simultaneously inhibiting three pivotal enzymes involved in AA metabolism, namely COX-2, 15-LOX and PGES-1. Indeed, the ability of a single compound to act on different targets involved in the same signalling pathway may lead to a fine-tuning of this pathological process, allowing the dosage of the drug to be reduced. In general, all the newly synthesized compounds proved to inhibit COX enzymes, displaying a clear preference for the less ulcerogenic COX-2 isoform, with a potency comparable to the marketed drug celecoxib. They also showed a remarkable inhibitory activity on 15-LOX, even better than the reference quercetin. In addition, compounds **2a-c**, by also inhibiting mPGES-1, acted as triple enzyme inhibitors, showing great promise as new anti-inflammatory agents.

From a structural point of view, compounds **2a-c**, bearing a large and lipophilic benzyl group in the hydrazone-carbamate function, proved to be the most potent on the three selected targets, probably due to their ability to establish significant hydrophobic interactions with peculiar aminoacids located in the pockets of the three enzymes. The only exception was the methylcarbazate derivative **1a**, which significantly inhibited all the selected targets despite a reduced COX-1/COX-2 SI. The methoxy substituent on the chromone moiety was seen to play a minor role in the potency against COXs and 15-LOX. Regarding mPGES-1 inhibition, for which the only data available refer to the methylcarbazate **1a** and the benzylcarbazate series **2a-c**, the role of the methoxy appeared more significant: the 7-methoxy derivative (**2c)** was 1.75 and 1.40 fold more active than the 6-methoxy-substituted **2b** and the unsubstituted **2a**, respectively.

In the cellular assay, the selected derivatives **2a-c** showed a similar profile, being able to reduce pro-inflammatory mediators and increase the anti-inflammatory cytokine IL-10 to similar levels as celecoxib. This behaviour was confirmed in *in vivo* studies, since a reduction in the rat paw edema to a comparable extent with both celecoxib and diclofenac was observed.

Compounds **2a-c** could thus be regarded as multipotent anti-inflammatory prototypes, able to interfere with different steps of the AA cascade. Moreover, the favourable modulation of COX-1/COX-2 selectivity could allow to lower the risk of the cardiovascular side effects, often observed with the highly selective COX-2 inhibition of the marketed coxibs.

5. Experimental section

5.1. Chemistry

General Methods. All chemicals were purchased from Aldrich Chemistry, Milan (Italy), or Alfa Aesar, Milan (Italy), and were of the highest purity. The selected solvents were of analytical grade. Thin layer chromatography (TLC) on precoated silica gel plates (Merck Silica Gel 60 F254) was applied to monitor reaction progress, and then visualized with a UV254 lamplight. Compounds purifications were performed by flash chromatography on silica gel columns (Kieselgel 40, 0.040–0.063 mm, Merck). Melting points were determined in open glass capillaries, using a Büchi apparatus and are uncorrected. ^{1}H NMR spectra were recorded for the intermediated compounds on a Varian Gemini spectrometer working at 400 MHz, while for the final compounds ^{1}H NMR and ^{13}C NMR spectra were recorded on a Bruker spectrometer working at 600 MHz and at 150 MHz, respectively, in DMSO-d_6 solutions unless otherwise indicated. Chemical shifts (δ) were reported as parts per million (ppm) values relative to tetramethylsilane (TMS) as internal standard; coupling constants (J) are reported in Hertz (Hz). Standard abbreviations were used for indicating spin multiplicities: s (singlet), d (doublet), dd (double doublet), t (triplet), br (broad), q (quartet) or m (multiplet). HRMS spectra were recorded on a Waters Xevo G2-XS quadrupole time-of-flight apparatus operating in electrospray mode. UHPLC−MS analyses were run on a Waters ACQUITY ARC UHPLC/MS system, consisting of a QDa mass spectrometer equipped with an electrospray ionization interface and a 2489 UV/Vis detector at wavelengths (λ) 254 nm and 365 nm. The analyses were performed on an XBridge BEH C18 column (10 × 2.1 mm i.d., particle size 2.5 μm) with a XBridge BEH C18 VanGuard Cartridge precolumn (5 mm × 2.1 mm i.d., particle size 1.8 μm), with mobile phases consisting in H_2O (0.1 % formic acid) (A) and MeCN (0.1 % formic acid) (B). Electrospray (ES) ionization in positive and negative modes was applied in the mass scan range of 50–1200 Da. Method and gradients used were the following: Generic method. Linear gradient: 0−0.78 min, 20 % B; 0.78–2.87 min, 20−95 % B; 2.87–3.54 min, 95 % B; 3.54–3.65 min, 95-20 % B; 3.65-5-73, 20 % B. Flow rate: 0.8 mL/min. All tested compounds were found to have >95 % purity. Compounds were named relying on the naming algorithm

developed by CambridgeSoft Corporation and used in ChemBioDraw Ultra (version 20.1).

5.1.1. General methods for the preparation of 4-oxo-4H-chromene-3-carbaldehyde derivatives (4b-c)

A solution of anhydrous *N*,*N*-dimethylformamide (12 mL) was heated at 50 °C and $POCl_3$ (5 eq) was slowly added. The solution was stirred for 2h, then the selected acetophenone (2-hydroxy-4-methoxyacetophenone and 2-hydroxy-5-methoxyacetophenone, 1 eq) was added dropwise. The mixture was heated at 60–70 °C for 4h, left at rt overnight, and then poured into ice/water (40 mL). The crude product was filtered under *vacuum* and washed with water.

5.1.2. 6-Methoxy-4-oxo-4H-chromene-3-carbaldehyde (4b)

Starting from 1-(2-hydroxy-5-methoxyphenyl)ethan-1-one (1.34 g, 8.7 mmol), 0.9 g of the desired compound were obtained (55 %). Mp 162–163 °C (lit. 164–166 °C, [39]. ^{1}HNMR: δ 3.94 (s, 3H, OCH_3), 7.33 (dd, J = 3.2 and 8.8 Hz, 1H, Ar),7.48 (d, J = 9.6 Hz,1H, Ar), 7.65 (d, J = 2.4 Hz, 1H, Ar), 8.54 (s, 1H, CH–O), 10.41 (s, 1H, CHO).

5.1.3. 7-Methoxy-4-oxo-4H-chromene-3-carbaldehyde (4c)

Starting from 1-(2-hydroxy-4-methoxyphenyl)ethan-1-one (1.34 g, 8.7 mmol), 1.05 g of the corresponding aldehyde were obtained (64 %). Mp 176–178 °C. ^{1}HNMR: δ 3.94 (s, 3H, OCH_3), 6.92 (d, J = 2.4 Hz, 1H, Ar), 7.05 (dd, J = 2.4 and 8.8 Hz, 1H, Ar), 8.21 (d, J = 8.8 Hz, 1H, Ar), 8.49 (s, 1H, CH–O), 10.39 (s, 1H, CHO) [58].

5.1.4. General procedure for the synthesis of N-acylhydrazone derivatives (1a-c, 2a-c, 3a-c)

The selected hydrazine-derivative (methyl hydrazinecarboxylate, benzyl hydrazinecarboxylate or methylhydrazine, 1 eq) was dissolved in ethanol, and the appropriately selected substituted formyl chromone (1 eq) was added portion-wise. The mixture was refluxed 1h, cooled at rt and the formed solid was collected by filtration. The final compounds were purified by recrystallization from ethanol.

5.1.5. Methyl (E)-2-((4-oxo-4H-chromen-3-yl)methylene)hydrazine-1-carboxylate (1a)

Using the previous procedure, starting from 0.3 g of **4a** and 0.16 g of methylcarbazate, 0.41 g of **1a** were obtained (97 %). The compound was recrystallized from ethanol [38]. Mp 206–210 °C. ^{1}H NMR: δ 3.68 (s, 3H, OCH_3), 7.52–7.56 (m, 1H, Ar), 7.69-7-72 (m, 1H, Ar), 7.82–7.87 (m, 1H, Ar), 8.09–8.12 (m, 1H, Ar), 8.17 (s, 1H, CH=N), 8.70 (s, 1H, CH–O), 11.21 (s, 1H, NH).^{13}C NMR: δ 52.01 (1C, OCH_3), 118.39 (1C, Ar), 118.73 (1C, Ar), 123.31 (1C, Ar), 125.21 (1C, Ar), 126.06 (1C, CH=N), 134.68 (2C, Ar), 154.02 (2C, Ar), 155.79 (1C, $COOCH_3$), 175.03 (1C, C=O). MS (ES) *m/z*: 269 (M + Na). HRMS *m/z*: [M+Na]: calcd. for $C_{12}H_{10}N_2NaO_4$ 269.05383; found 269.05286.

5.1.6. Methyl (E)-2-((6-methoxy-4-oxo-4H-chromen-3-yl)methylene) hydrazine-1-carboxylate (1b)

Using the previous procedure, starting from 0.3 g of **4b** and 0.13 g of methylcarbazate, 0.41 g of **1b** were obtained (51 %). The compound was recrystallized from ethanol. Mp 213–214 °C. ^{1}H NMR: δ 3.68 (s, 3H, $COOCH_3$), 3.87 (s, 3H, OCH_3), 7.44 (dd, 1H, J = 9.1, 3.1 Hz, Ar), 7.47 (d, 1H, J = 3.1 Hz, Ar), 7.68 (d, 1H, J = 9.1 Hz, Ar), 8.19 (s, 1H, CH=N), 8.69 (s, 1H, CH–O), 11.19 (s, 1H, NH). ^{13}C NMR: δ 52.01 (1C, OCH_3), 55.86 (1C, OCH_3), 104.93 (1C, Ar), 117.58 (1C, Ar), 120.38 (1C, Ar), 123.73 (2C, Ar), 124.05 (CH=N), 150.57 (1C, Ar), 153.78 (1C, $COOCH_3$), 156.96 (2C, Ar), 174.74 (1C, C=O). MS (ES) *m/z*: 277.02 (M + H). HRMS *m/z*: [M+Na]: calcd. for $C_{13}H_{12}N_2NaO_5$ 299.0643; found 299.0637.

5.1.7. Methyl (E)-2-((7-methoxy-4-oxo-4H-chromen-3-yl)methylene) hydrazine-1-carboxylate (1c)

Using the previous procedure, starting from 0.29 g of **4c** and 0.13 g of methylcarbazate, 0.14 g of **1c** were obtained (40 %). The compound was recrystallized from ethanol. Mp 228–229 °C. ^{1}H NMR: δ 3.68 (s, 3H, $COOCH_3$), 3.90 (s, 3H, OCH_3), 7.10 (dd, 1H, J = 8.9, 2.40 Hz, Ar), 7.19 (d, 1H, J = 2.4 Hz, Ar), 8.00 (d, 1H, J = 8.9 Hz, Ar), 8.15 (s, 1H, CH=N), 8.63 (s, 1H, CH–O), 11.19 (s, 1H, NH). ^{13}C NMR: δ 52.01 (1C, OCH_3), 56.25 (1C, OCH_3), 101.05 (1C, Ar), 115.32 (1C, Ar), 117.02 (1C, Ar), 118.22 (2C, Ar), 126.66 (1C, C=NH), 153.51 (1C, $COOCH_3$), 157.68 (2C, Ar), 164.14 (1C, Ar), 174.29 (1C, C=O). MS (ES) *m/z*: 277.12 (M + H). HRMS *m/z*: [M+Na]: calcd. for $C_{13}H_{12}N_2NaO_5$ 299.0643; found 299.0633.

5.1.8. Benzyl (E)-2-((4-oxo-4H-chromen-3-yl)methylene)hydrazine-1-carboxylate (2a)

Using the previous procedure, starting from 0.3 g of **4a** and 0.29 g of benzylcarbazate, 0.52 g of **2a** were obtained (94 %). The compound was recrystallized from ethanol. Mp 218–220 °C. ^{1}H NMR: δ 5.17 (s, 2H, CH_2), 7.34–7.38 (m, 1H, Ar C_6H_5), 7.38–7.41 (m, 4H, C_6H_5), 7.52–7.55 (m, 1H, Ar), 7.68–7.72 (m, 1H, Ar), 7.82–7.87 (m, 1H, Ar), 8.10 (dd, 1H, J = 8.0, 1.6 Hz), 8.12 (s, 1H, CH=N), 8.71 (s, 1H, CH–O), 11.37 (s, 1H, NH). ^{13}C NMR: δ 66.05 (CH_2), 118.41 (1C, Ar), 118.76 (1C, Ar), 123.33 (1C, Ar), 125.24 (1C, Ar), 126.10 (1C, Ar), 128.05 (2C, Ar), 128.15 (1C, Ar), 128.53 (2C, Ar), 134.72 (2C, Ar), 136.56 (CH=NH), 154.15 (1C, $COOCH_2C_6H_5$), 155.82 (2C, Ar), 175.05 (1C, C=O). MS (ES) *m/z*: 323.14 (M + H). HRMS *m/z*: [M+Na]: calcd. for $C_{18}H_{14}N_2NaO_4$ 345.0851; found 345.0841.

5.1.9. Benzyl (E)-2-((6-methoxy-4-oxo-4H-chromen-3-yl)methylene) hydrazine-1-carboxylate (2b)

Using the previous procedure, starting from 0.3 g of **4b** and 0.24 g of benzylcarbazate, 0.26 g of **2a** were obtained (50 %). The compound was recrystallized from ethanol. Mp 204–211 °C. ^{1}H NMR: δ 3.87 (s, 3H, OCH_3), 5.17 (s, 2H, CH_2), 7.32–7.37 (m, 1H, Ar), 7.37–7.43 (m, 4H, Ar), 7.44 (dd, 1H, J = 9.00, 3.1 Hz, Ar), 7.46 (d, 1H, J = 3.1 Hz, Ar), 7.68 (d, 1H, J = 9.1 Hz, Ar), 8.19 (s, 1H, CH=N), 8.69 (s, 1H, CH–O), 11.34 (s, 1H, NH). ^{13}C NMR: δ 55.82 (1C, OCH_3), 65.93 (1C, CH_2), 104.90 (1C, Ar), 117.55 (1C, Ar), 120.33 (1C, Ar), 123.68 (1C, Ar), 124.03 (1C, Ar), 127.98 (3C, Ar), 128.06 (1C, Ar), 128.46 (2C, Ar), 136.53 (1C, CH=NH), 150.53 (1C, Ar), 153.79 (1C, $COOCH_2C_6H_5$), 156.92 (2C, Ar), 174.67 (1C, C=O). MS (ES) *m/z*: 353.25 (M + H). HRMS *m/z*: [M+Na]: calcd. for $C_{19}H_{16}N_2NaO_5$ 375.0956; found 375.0947.

5.1.10. Benzyl (E)-2-((7-methoxy-4-oxo-4H-chromen-3-yl)methylene) hydrazine-1-carboxylate (2c)

Using the previous procedure, starting from 0.3 g of **4c** and 0.24 g of benzylcarbazate, 0.28 g of **2c** were obtained (54 %). The compound was recrystallized from ethanol. Mp 217–218 °C. ^{1}H NMR: δ 3.90 (s, 3H, OCH_3), 5.17 (s, 2H, CH_2), 7.10 (dd, 1H, J = 8.9, 2.4 Hz, Ar), 7.20 (d, 1H, J = 2.4 Hz, 1H, Ar), 7.32–7.38 (m, 1H, Ar), 7.38–7.43 (m, 4H, Ar), 8.00 (d, 1H, J = 1.9 Hz, Ar), 8.16 (s, 1H, CH=N), 8.63 (s, 1H, CH–O), 11.34 (s, 1H, NH). ^{13}C NMR: δ 56.21 (1C, OCH_3), 65.94 (1C, CH_2), 101.02 (2C, Ar), 115.26 (1C, Ar), 116.99 (1C, Ar), 118.18 (1C, Ar), 126.60 (1C, Ar), 127.97 (2C, Ar), 128.06 (1C, Ar), 128.45 (2C, Ar), 136.53 (1C, CH=NH), 153.51 (1C, $COOCH_2C_6H_5$), 157.63 (2C, Ar), 164.09 (1C, Ar), 174.20 (1C, C=O). MS (ES) *m/z*: 353.25 (M + H). HRMS *m/z*: [M+Na]: calcd. for $C_{19}H_{16}N_2NaO_5$ 375.0956; found 375.0949.

5.1.11. (E)-3-((2-methylhydrazineylidene)methyl)-4H-chromen-4-one (3a)

Using the previous procedure, starting from 0.5 g of **4a** and 0.15 g of methylhydrazine, 0.25 g of **3a** were obtained (44 %). The compound was recrystallized from ethanol. Mp 69–70 °C. ^{1}H NMR: δ 3.11 (s, 3H, CH_3), 6.96 (td, 1H, J = 7.4, 1.1 Hz, Ar), 6.99 (dd, 1H, J = 8.3, 1.1 Hz, Ar), 7.44–7.48 (m, 1H, Ar), 7.67 (dd, 1H, J = 7.8, 1.7 Hz, Ar), 7.93 (s, 1H, CH=N), 8.36 (s, 1H, CH–O), 11.13 (s, 1H, NH). ^{13}C NMR: δ 38.83 (1C, CH_3) 117.24 (1C, Ar), 119.13 (1C, Ar), 121.86 (1C, Ar), 123.36 (1C, Ar), 130.30 (1C, Ar), 134.02 (1C, Ar), 135.30 (1C, CH=N), 140.82 (1C,

Ar), 158.61 (1C, Ar), 190.18 (1C, C=O). MS (ES) *m/z*: 203.20 (M + H). HRMS *m/z*: [M+H]: calcd. for $C_{11}H_{11}N_2O_2$ 203.0821; found 203.0809.

5.1.12. (E)-6-Methoxy-3-((2-methylhydrazineylidene)methyl)-4H-chromen-4-one (3b)

Using the previous procedure, starting from 0.3 g of **4b** and 0.078 g of methylhydrazine, 0.17 g of **3b** were obtained (56 %). The compound was recrystallized from ethanol. Mp 82–86 °C. ^{1}H NMR (DMSO): δ 3.74 (s, 3H, COOCH_3), 3.91 (s, 3H, COCH_3), 6.92 (dt, 1H, J = 9.4, 1.6 Hz, Ar), 7.07 (s, 1H, Ar), 7.05–7.09 (m, 1H, Ar), 7.92 (s, 1H, CH=N), 8.35 (s, 1H, CH–O), 10.43 (s, 1H, NH). ^{13}C NMR (DMSO): δ 38.83 (1C, CH_3), 55.52 (1C, OCH_3), 113.37 (1C, Ar), 118.15 (1C, Ar), 120.56 (1C, Ar), 122.04 (1C, Ar), 123.91 (1C, Ar), 135.29 (1C, CH=N), 140.78 (1C, Ar), 151.67 (1C, Ar), 151.95 (1C, Ar), 189.60 (1C, C=O). MS (ES) *m/z*: 233.21 (M + H). HRMS *m/z*: [M+H]: calcd. for $C_{12}H_{13}N_2O_3$ 233.0926; found 233.0916.

5.1.13. (E)-7-Methoxy-3-((2-methylhydrazineylidene)methyl)-4H-chromen-4-one (3c)

Using the previous procedure, starting from 0.6 g of **4c** and 0.16 g of methylhydrazine, 0.33 g of **3c** were obtained (96 %). The compound was recrystallized from ethanol. Mp 131–133 °C. ^{1}H NMR: δ 3.83 (s, 3H, COOCH_3), 3.92 (s, 3H, COCH_3), 6.53 (d, 1H, J = 2.5 Hz, Ar), 6.55 (dd, 1H, J = 8.8, 2.6 Hz, Ar), 7.86 (d, 1H, J = 8.9 Hz, Ar), 7.98 (s, 1H, CH=N), 8.44 (s, 1H, CH–O), 12.61 (s, 1H, NH). ^{13}C NMR: δ 38.91 (1C, CH_3), 55.73 (1C, OCH_3), 101.23 (1C, Ar), 107.25 (1C, Ar), 114.00 (1C, Ar), 120.93 (1C, Ar), 133.07 (1C, Ar), 134.87 (1C, CH=N), 140.73 (1C, Ar), 164.22 (1C, Ar), 165.20 (1C, Ar), 189.97 (1C, C=O). MS (ES) *m/z*: 233.21 (M + H). HRMS *m/z*: [M+H]: calcd. for $C_{12}H_{13}N_2O_3$ 233.0926; found 233.0916.

5.2. Biological evaluation

5.2.1. In vitro COX-1/2 and 15-LOX inhibition assays

The inhibitory activity of test compounds against COX-1 and COX-2 was assessed using Cayman colorimetric COX (ovine) inhibitor screening assay kit (Catalog No. 560131), while the inhibitory activity against soya bean 15-LOX was assessed using Cayman lipoxygenase inhibitor screening assay kit (catalog No. 760700), both supplied by Cayman chemicals, Ann Arbor, MI, USA. The preparation of reagents and testing procedures for determining IC_{50} values of the tested compounds were carried out following the manufacturer's instructions and in agreement with our previous work [21,59].

5.2.2. In vitro mPGE2 synthase-1 inhibitory assay

Microsomal preparation of interleukin-1β-stimulated human lung carcinoma A549 has been used as a source of mPEGS-1 for the assessment of the activity of the inhibitors in a cell free assay, as previously reported [46]. PGH2 substrate (Catalogue number 17020, Cayman Chemicals, Ann Arbor, MI, USA, 20 μM) and serial dilutions of the inhibitors were added to reaction mixture containing glutathione (2.5 mM) and mPEGS-1 microsomal preparations. After 5 min at room temperature, the reaction was stopped by converting the remaining PGH2 to PGF2α using $SnCl_2$, and the formed PGE2 is quantified by PGE2 ELISA assay kit (Catalogue number 514010, Cayman Chemicals, Ann Arbor, MI, USA) following the manufacturer's instructions. A dose response curve was established between PGE2 concentrations and the inhibitor logarithmic concentrations from which $IC_{50} \pm$ SD was determined using GraphPad Prism.

5.2.3. In vivo experiments

This study was conducted according to an animal handling protocol approved by our Institutional Animal Care and Use Committee and following the Guide for the Care and Use of Laboratory Animals published by the US National Institute of Health (NIH publication No. 83–23, revised 1996). Animals were provided the appropriate care throughout all experiments to reduce any discomfort or pain. Adult female Wistar rats, weighing 150–250 g, were obtained from Alexandria University Experimental Animal Centre. They were kept in a controlled setting at a temperature of 23–25 °C with a 12 h dark/light cycle, and allowed access to food and water *ad libitum*. Prior to the trial, rats had a 7-day acclimatization period. Animals were randomly divided into six groups (six rats each), the control sets received the vehicle only (DMSO), two reference sets were treated with either celecoxib (5 mg/kg) or diclofenac sodium (5 mg/kg) as reference anti-inflammatory compounds (both from European Egyptian Pharmaceutical Industries, Alexandria, Egypt), while the three test groups received one of compounds **2a-c** (5 mg/kg). All drugs were dissolved in DMSO and given orally by gastric gavage once daily for seven consecutive days. Both the ulcerogenicity experiments and the inflammatory models used the same groups of rats.

5.2.3.1. Formalin-induced paw edema test (acute inflammation model).

The formalin-induced paw edema protocol [60,61], was used as an acute inflammatory model for the *in vivo* evaluation of the anti-inflammatory effect of the test compounds. As a phlogistic agent, 5 % formalin solution was used. It was freshly prepared from 37 % formaldehyde and saline (Merck, Germany). On the eighth day, a Vernier calliper was used to calculate the initial paw volume. Following that, all groups received a subcutaneous injection of 40 μL formalin into their right hind paws while being lightly anaesthetized with ether. After 4 h, the paw volume was measured, and the edema volume was determined through calculating the difference in paw volume before and after the formalin injection.

5.2.3.2. Gastric ulcerogenic activity and histopathological studies.

After eight days of treatment with the compounds, the rat stomachs were removed, and processed for gross and histological observation of ulcerative signs as described previously [24,62,63].

5.2.4. In vitro assessment of the effect of reference and test compounds on the expression of inflammatory mediators triggered by macrophage exposure to lipopolysaccharides

The *in vitro* anti-inflammatory effect of the test compounds was determined by examining their effect on the expression of COX-2, iNOS, IL-1β, TNF-α, and IL-10 in Lipopolysaccharides (Sigma-Aldrich, St. Louis, MO, USA) (LPS)-challenged RAW264.7 macrophage cells (Shanghai BOGO Industrial Co., Ltd., Shanghai, China) as described previously [64]. RAW264.7 cells in logarithmic growth phase were cultured in Dulbecco's modified Eagle's medium (DMEM) supplemented with 10 % fetal bovine serum (FBS) (General Electric Healthcare Life Sciences, Mississauga, Canada), containing 1 % Penicillin streptomycin (P/S 100 U/ml and 100 mg/ml, respectively, Solarbio life sciences, Beijing, P. R. China) at 37 °C and 5 % CO_2. To determine the effect of each of the compounds used in this study on cell viability, RAW264.7 macrophage cells were seeded into 96 well plates at a concentration of 4 $\times$ 10^3 cells per well, with different concentrations (100 μg/ml to 0.4 μg/ml) of the compounds used dissolved in DMSO and incubated for 72 h. Subsequently, a solution of 5 mg/ml 3-(4,5-dimethylthiazol-2-yl)-2, 5-diphenyltetrazolium bromide (MTT; Sigma-Aldrich) was added to each well and then incubated at 37 °C in the presence of 5 % CO_2 for 4 h. After incubation, the supernatant was removed and DMSO was added to dissolve formazan. Finally, a UV MAX kinetic microplate reader (Molecular Devices, LLC) was used to measure the absorbance at 490 nm, which was corresponding to cell metabolic activity. The highest drug concentration maintaining above 80 % cell activity was used for the next step.

To determine the effect of different compounds on inflammatory mediators, RAW264.7 macrophage cells were seeded in 24-well plates at a density of 4 $\times$ 10^5 per well. Cells were incubated with the different compounds and 1 μg/ml LPS for 24 h. Afterwards, cells were washed

once with PBS (1 mL/well). Cell lysates were prepared by exposing cell monolayers to 200 mL/well of Bio-Rad iScript Sample Preparation Reagent (referred to as Bio-Rad SPR; 170–8898) or Cell-Lysis (CL) Buffer. The final formulation of CL Buffer consisted of 10 mM Tris-HCl pH 7.4, 0.25 % Igepal CA-630, and 150 mM NaCl. CL Buffer was freshly prepared from the following stock solutions on the day of experimentation: 1 M Tris-HCl (T2194; Sigma), 10 % Igepal CA-630 (I8896; Sigma); and 5 M NaCl (351-036-100; Quality Biological, Inc.). All reagents were molecular biology grade and dilutions were made with DEPC-treated water (351-068-721; Quality Biological, Inc.). CL Buffer also included $MgCl_2$ (M1028; Sigma) or RNasin Plus RNase Inhibitor (N2615; Promega). Both Bio-Rad SPR and CL Buffer were equilibrated to room temperature prior to use. Cells were exposed for the indicated times (typically 2 min for Bio-Rad SPR and 5 min for CL Buffer). The resulting lysates were carefully collected without disturbing the cell-monolayer remnants and analyzed immediately. The expression levels of inflammatory mediators were determined using real time quantitative polymerase chain reaction (RT-qPCR) assays. RT-qPCR analysis was performed in one-step SYBR Green RT-qPCR. Each reaction contained: template (1 mL of cell lysate), iScript One-Step SYBR Green RT-PCR Supermix (170–8893; Bio-Rad), 600 nM of each primer (synthesized at the Facility for Biotechnology Resources; CBER, FDA; Bethesda, MD), and nuclease-free water to 10 mL. A CFX96 real-time PCR instrument (Bio-Rad) was used with the following protocol: 50 °C for 10 min, 95 °C for 5 min, 95 °C for 10 s/61 °C for 15 s/72 °C for 30 s. The primer used had the following sequences: COX-2 F 5′-GCGACATACTCAAGCAGGAGCA-3′, R 5′-AGTGGTAACCGCTCAGGTGTTG-3’; iNOS F 5′-GCTCTACACCTCCAATGTGACC-3′, R 5′-CTGCCGAGATTTGAGCCTCATG-3’; IL-1β F 5′-CCACAGACCTTCCAGGAGAATG-3′, R 5′-GTGCAGTTCAGTGATCGTACAGG-3’; TNF-α F 5′-CTCTTCTGCCTGCTGCACTTTG-3′, R 5′-ATGGGCTACAGGCTTGTCACTC-3’; IL-10 F 5′-CGGGAAGACAATAACTGCACCC-3′, R 5′-CGGTTAGCAGTATGTTGTCCAGC-3’; and β-actin F 5′-GCACCACACCTTCTACAATG-3′, R 5′-TGCTTGCTGATCCACATCTG-3’. Transcript abundance was computed by the $2^{-\Delta\Delta Ct}$ method with β-actin as a reference.

5.2.5. Statistical analysis

Unless otherwise indicated, data were expressed as mean ± standard error of the mean. Statistical significance was tested using the appropriate statistical test as indicated in the corresponding section in the results or the figure legends using GraphPad Prism software version 7. P value < 0.05 was considered statistically significant.

5.3. Molecular docking

As we previously reported [24,65,66]), MOE 2019.0102 software (Chemical Computing Group, Montreal, Canada) was used along with the crystal structures of mPGES1 (PDB 4AL1), COX-2 active site (PDB 1CX2) and 15-LOX active site (PDB 1LOX) to conduct the docking experiments. The database of the active compounds was appropriately handled *via* hydrogen atoms addition, partial charges calculation and Force Field MMFF94x assisted energy minimization. Also, irrelevant extra protein chains, water molecules and surfactant molecules were cleared out. We followed the default settings offered by MOE, which included triangle matcher as a placement method and London dG as a main scoring function followed by GBVI/WSA dG scoring function as a secondary refinement step. Guided by the scoring functions together with the visual inspection of the hydrophobic, ionic, and hydrogen-bond with the binding pocket residues, we picked the optimum poses that showed both the best score and interactions.

5.3.1. In silico prediction of pharmacokinetic profile, drug likeness and ligand efficiency parameters

We used Molinspiration online property calculation toolkit, PreADMET calculator, Pro TOX-II tool, SwissADME program and Datawarrior software to predict physicochemical properties, ADME, toxicity, drug likeness and ligand efficiency metrics of the most active compounds, respectively.

CRediT authorship contribution statement

Perihan A. Elzahhar: Data curation, Investigation, Writing – original draft. **Rebecca Orioli:** Data curation, Investigation, Methodology. **Nayera W. Hassan:** Formal analysis, Investigation, Visualization. **Silvia Gobbi:** Data curation, Validation, Writing – review & editing. **Federica Belluti:** Formal analysis, Validation. **Hala F. Labib:** Data curation, Methodology, Validation. **Ahmed F. El-Yazbi:** Investigation, Methodology, Supervision, Writing – review & editing. **Rasha Nassra:** Formal analysis, Methodology, Visualization. **Ahmed S.F. Belal:** Conceptualization, Funding acquisition, Supervision, Writing – review & editing, Project administration. **Alessandra Bisi:** Conceptualization, Funding acquisition, Project administration, Supervision, Writing – original draft.

Declaration of competing interest

The authors declare that they have no known competing financial interests or personal relationships that could have appeared to influence the work reported in this paper.

Data availability

Data will be made available on request.

Appendix A. Supplementary data

Supplementary data to this article can be found online at https://doi.org/10.1016/j.ejmech.2024.116138.

References

[1] S.E. Headland, L.V. Norling, The resolution of inflammation: principles and challenges, Semin. Immunol. 27 (2015) 149–160, https://doi.org/10.1016/j.smim.2015.03.014.
[2] L.C.F. Opretzka, R.F. do Espírito-Santo, O.A. Nascimento, L.S. Abreu, I.M. Alves, E. Döring, M.B.P. Soares, E. da S. Velozo, S.A. Laufer, C.F. Villarreal, Natural chromones as potential anti-inflammatory agents: pharmacological properties and related mechanisms, Int. Immunopharm. 72 (2019) 31–39, https://doi.org/10.1016/j.intimp.2019.03.044.
[3] G. Moussa, R. Alaaeddine, L.M. Alaeddine, R. Nassra, A.S.F. Belal, A. Ismail, A. F. El-Yazbi, Y.S. Abdel-Ghany, A. Hazzaa, Novel click modifiable thioquinazolinones as anti-inflammatory agents: design, synthesis, biological evaluation and docking study, Eur. J. Med. Chem. 144 (2018) 635–650, https://doi.org/10.1016/j.ejmech.2017.12.065.
[4] P.A. Elzahhar, R.A. Alaaeddine, R. Nassra, A. Ismail, H.F. Labib, M.G. Temraz, A.S. F. Belal, A.F. El-Yazbi, Challenging inflammatory process at molecular, cellular and in vivo levels via some new pyrazolyl thiazolones, J. Enzym. Inhib. Med. Chem. 36 (2021) 669–684, https://doi.org/10.1080/14756366.2021.1887169.
[5] R. De Simone, M.G. Chini, I. Bruno, R. Riccio, D. Mueller, O. Werz, G. Bifulco, Structure-based discovery of inhibitors of microsomal prostaglandin E $_2$ Synthase−1, 5-lipoxygenase and 5-lipoxygenase-activating protein: promising hits for the development of new anti-inflammatory agents, J. Med. Chem. 54 (2011) 1565–1575, https://doi.org/10.1021/jm101238d.
[6] P.A. Elzahhar, S.M. Abd El Wahab, M. Elagawany, H. Daabees, A.S.F. Belal, A.F. EL-Yazbi, A.H. Eid, R. Alaaeddine, R.R. Hegazy, R.M. Allam, M.W. Helmy, Bahaa Elgendy, A. Angeli, S.A. El-Hawash, C.T. Supuran, Expanding the anticancer potential of 1,2,3-triazoles via simultaneously targeting Cyclooxygenase-2, 15-lipoxygenase and tumor-associated carbonic anhydrases, Eur. J. Med. Chem. 200 (2020) 112439, https://doi.org/10.1016/j.ejmech.2020.112439.
[7] B. Wang, L. Wu, J. Chen, L. Dong, C. Chen, Z. Wen, J. Hu, I. Fleming, D.W. Wang, Metabolism pathways of arachidonic acids: mechanisms and potential therapeutic targets, Signal Transduct. Targeted Ther. 6 (2021) 94, https://doi.org/10.1038/s41392-020-00443-w.
[8] R.A. Alaaeddine, P.A. Elzahhar, I. AlZaim, W. Abou-Kheir, A.S.F. Belal, A.F. El-Yazbi, The emerging role of COX-2, 15-LOX and PPARγ in metabolic diseases and cancer: an introduction to novel multi-target directed ligands (MTDLs), Curr. Med. Chem. 28 (2020) 2260–2300, https://doi.org/10.2174/0929867327999200820173853.
[9] P. Asadi, M. Alvani, V. Hajhashemi, M. Rostami, G. Khodarahmi, Design, synthesis, biological evaluation, and molecular docking study on triazine based derivatives as

anti-inflammatory agents, J. Mol. Struct. 1243 (2021) 130760, https://doi.org/10.1016/j.molstruc.2021.130760.
[10] J.P. Peesa, P.R. Yalavarthi, A. Rasheed, V.B.R. Mandava, A perspective review on role of novel NSAID prodrugs in the management of acute inflammation, Journal of Acute Disease 5 (2016) 364–381, https://doi.org/10.1016/j.joad.2016.08.002.
[11] F. Buttgereit, G.R. Burmester, L.S. Simon, Gastrointestinal toxic side effects of nonsteroidal anti-inflammatory drugs and cyclooxygenase-2–specific inhibitors, Am. J. Med. 110 (2001) 13–19, https://doi.org/10.1016/S0002-9343(00)00728-2.
[12] P. Ungprasert, N. Srivali, W. Kittanamongkolchai, Non-steroidal anti-inflammatory drugs and risk of heart failure exacerbation: a systematic review and meta-analysis, Eur. J. Intern. Med. 26 (2015) 685–690, https://doi.org/10.1016/j.ejim.2015.09.012.
[13] D. Claveau, M. Sirinyan, J. Guay, R. Gordon, C.-C. Chan, Y. Bureau, D. Riendeau, J. A. Mancini, Microsomal prostaglandin E synthase-1 is a major terminal synthase that is selectively up-regulated during cyclooxygenase-2-dependent prostaglandin E2 production in the rat adjuvant-induced arthritis model, J. Immunol. 170 (2003) 4738–4744, https://doi.org/10.4049/jimmunol.170.9.4738.
[14] K. Yoshimatsu, D. Golijanin, P.B. Paty, R.A. Soslow, P.-J. Jakobsson, R.A. DeLellis, K. Subbaramaiah, A.J. Dannenberg, P.R. A D, P.R. A S, Inducible microsomal prostaglandin E synthase is overexpressed in colorectal adenomas and cancer, Clin. Cancer Res. 7 (2001) 3971–3976. http://aacrjournals.org/clincancerres/article-pdf/7/12/3971/2079714/df1201003971.pdf.
[15] S. Mehrotra, A. Morimiya, B. Agarwal, R. Konger, S. Badve, Microsomal prostaglandin E2 synthase-1 in breast cancer: a potential target for therapy, J. Pathol. 208 (2006) 356–363, https://doi.org/10.1002/path.1907.
[16] Q. Wang, Y. Li, M. Wu, S. Huang, A. Zhang, Y. Zhang, Z. Jia, Targeting microsomal prostaglandin E synthase 1 to develop drugs treating the inflammatory diseases, Am. J. Tourism Res. 13 (2021) 391–419.
[17] H. Sadeghian, A. Jabbari, 15-Lipoxygenase inhibitors: a patent review, Expert Opin. Ther. Pat. 26 (2016) 65–88, https://doi.org/10.1517/13543776.2016.1113259.
[18] R.G. Snodgrass, B. Brüne, Regulation and functions of 15-lipoxygenases in human macrophages, Front. Pharmacol. 10 (2019), https://doi.org/10.3389/fphar.2019.00719.
[19] J.A. Chandrasekharan, N. Sharma-Wali, Lipoxins: nature's way to resolve inflammation, J. Inflamm. Res. 8 (2015) 181–192, https://doi.org/10.2147/JIR.S90380.
[20] S. Feltenmark, N. Gautam, Åsa Brunnström, W. Griffiths, L. Backman, C. Edenius, L. Lindbom, M. Björkholm, H.-E. Claesson, Eoxins are proinflammatory arachidonic acid metabolites produced via the 15-lipoxygenase-1 pathway in human eosinophils and mast cells, Proc. Natl. Acad. Sci. USA 105 (2008) 680–685, https://doi.org/10.1073/pnas.0710127105.
[21] P.A. Elzahhar, R. Alaaeddine, T.M. Ibrahim, R. Nassra, A. Ismail, B.S.K. Chua, R. L. Frkic, J.B. Bruning, N. Wallner, T. Knape, A. von Knethen, H. Labib, A.F. El-Yazbi, A.S.F. Belal, Shooting three inflammatory targets with a single bullet: novel multi-targeting anti-inflammatory glitazones, Eur. J. Med. Chem. 167 (2019) 562–582, https://doi.org/10.1016/j.ejmech.2019.02.034.
[22] J.A. Ackermann, K. Hofheinz, M.M. Zaiss, G. Krönke, The double-edged role of 12/15-lipoxygenase during inflammation and immunity, Biochim. Biophys. Acta Mol. Cell Biol. Lipids (2017) 371–381, https://doi.org/10.1016/j.bbalip.2016.07.014, 1862.
[23] K. Liaras, M. Fesatidou, A. Geronikaki, Thiazoles and thiazolidinones as COX/LOX inhibitors, Molecules 23 (2018) 685, https://doi.org/10.3390/molecules23030685.
[24] P.A. Elzahhar, R.A. Alaaeddine, R. Nassra, A. Ismail, H.F. Labib, M.G. Temraz, A.S. F. Belal, A.F. El-Yazbi, Challenging inflammatory process at molecular, cellular and in vivo levels via some new pyrazolyl thiazolones, J. Enzym. Inhib. Med. Chem. 36 (2021) 669–684, https://doi.org/10.1080/14756366.2021.1887169.
[25] J. Cui, J. Jia, Natural COX-2 inhibitors as promising anti-inflammatory agents: an update, Curr. Med. Chem. 28 (2020) 3622–3646, https://doi.org/10.2174/0929867327999200917150939.
[26] C.F.M. Silva, D.C.G.A. Pinto, A.M.S. Silva, Chromones: a promising ring system for new anti-inflammatory drugs, ChemMedChem 11 (2016) 2252–2260, https://doi.org/10.1002/cmdc.201600359.
[27] R. Gautam, S.M. Jachak, V. Kumar, C.G. Mohan, Synthesis, biological evaluation and molecular docking studies of stellatin derivatives as cyclooxygenase (COX-1, COX-2) inhibitors and anti-inflammatory agents, Bioorg. Med. Chem. Lett 21 (2011) 1612–1616, https://doi.org/10.1016/j.bmcl.2011.01.116.
[28] S. Xie, S. Li, J. Tian, F. Li, Iguratimod as a new drug for rheumatoid arthritis: current landscape, Front. Pharmacol. 11 (2020), https://doi.org/10.3389/fphar.2020.00073.
[29] K. Rullah, M.F.F. Mohd Aluwi, B.M. Yamin, M.S. Baharuddin, N.H. Ismail, H. Y. Teruna, S.N.A. Bukhari, I. Jantan, J. Jalil, K. Husain, L.K. Wai, Molecular characterization, biological activity, and in silico study of 2-(3,4-dimethoxyphenyl)-3-(4-fluorophenyl)-6-methoxy-4H-chromen-4-one as a novel selective COX-2 inhibitor, J. Mol. Struct. 1081 (2015) 51–61, https://doi.org/10.1016/j.molstruc.2014.10.004.
[30] C.D. Sadik, H. Sies, T. Schewe, Inhibition of 15-lipoxygenases by flavonoids: structure–activity relations and mode of action, Biochem. Pharmacol. 65 (2003) 773–781, https://doi.org/10.1016/S0006-2952(02)01621-0.
[31] M. Hämäläinen, R. Nieminen, M. Asmawi, P. Vuorela, H. Vapaatalo, E. Moilanen, Effects of flavonoids on prostaglandin E $_2$ production and on COX-2 and mPGES-1 expressions in activated macrophages, Planta Med. 77 (2011) 1504–1511, https://doi.org/10.1055/s-0030-1270762.
[32] S. Thota, D.A. Rodrigues, P. de S.M. Pinheiro, L.M. Lima, C.A.M. Fraga, E. J. Barreiro, N-Acylhydrazones as drugs, Bioorg. Med. Chem. Lett 28 (2018) 2797–2806, https://doi.org/10.1016/j.bmcl.2018.07.015.
[33] L.-I. Socea, S.-F. Barbuceanu, E.M. Pahontu, A.-C. Dumitru, G.M. Nitulescu, R. C. Sfetea, T.-V. Apostol, Acylhydrazones and their biological activity: a review, Molecules 27 (2022) 8719, https://doi.org/10.3390/molecules27248719.
[34] T. de Melo, R. Chelucci, M. Pires, L. Dutra, K. Barbieri, P. Bosquesi, G. Trossini, M. Chung, J. dos Santos, Pharmacological evaluation and preparation of nonsteroidal anti-inflammatory drugs containing an N-acyl hydrazone subunit, Int. J. Mol. Sci. 15 (2014) 5821–5837, https://doi.org/10.3390/ijms15045821.
[35] H. Azizian, Z. Mousavi, H. Faraji, M. Tajik, K. Bagherzadeh, P. Bayat, A. Shafiee, A. Almasirad, Arylhydrazone derivatives of naproxen as new analgesic and anti-inflammatory agents: design, synthesis and molecular docking studies, J. Mol. Graph. Model. 67 (2016) 127–136, https://doi.org/10.1016/j.jmgm.2016.05.009.
[36] S.M. Noha, K. Fischer, A. Koeberle, U. Garscha, O. Werz, D. Schuster, Discovery of novel, non-acidic mPGES-1 inhibitors by virtual screening with a multistep protocol, Bioorg. Med. Chem. 23 (2015) 4839–4845, https://doi.org/10.1016/j.bmc.2015.05.045.
[37] T.A. Shaw, M.H. Powdrill, A.R. Sherratt, K. Garland, B.J. Li, A.M. Beauchemin, J. P. Pezacki, Reactivity of: N -acyl hydrazone probes with the mammalian proteome, RSC Med. Chem. 12 (2021) 797–803, https://doi.org/10.1039/d1md00027f.
[38] A. Łazarenkow, J. Nawrot-Modranka, E. Brzezińska, U. Krajewska, M. Różalski, Synthesis, preliminary cytotoxicity evaluation of new 3-formylchromone hydrazones and phosphorohydrazone derivatives of coumarin and chromone, Med. Chem. Res. 21 (2012) 1861–1868, https://doi.org/10.1007/s00044-011-9703-4.
[39] A. Nohara, T. Umetani, Y. Sanno, Studies on antianaphylactic agents—I, Tetrahedron 30 (1974) 3553–3561, https://doi.org/10.1016/S0040-4020(01)97034-6.
[40] G. Palla, G. Predieri, P. Domiano, C. Vignali, W. Turner, Conformational behaviour and/isomerization of -acyl and -aroylhydrazones, Tetrahedron 42 (1986) 3649–3654, https://doi.org/10.1016/S0040-4020(01)87332-4.
[41] R. Munir, N. Javid, M. Zia-ur-Rehman, M. Zaheer, R. Huma, A. Roohi, M.M. Athar, Synthesis of novel N-acylhydrazones and their C-N/N-N bond conformational characterization by NMR spectroscopy, Molecules 26 (2021) 4908, https://doi.org/10.3390/molecules26164908.
[42] A.L. Moraczewski, L.A. Banaszynski, A.M. From, C.E. White, B.D. Smith, Using hydrogen bonding to control carbamate C−N rotamer equilibria, J. Org. Chem. 63 (1998) 7258–7262, https://doi.org/10.1021/jo980644d.
[43] D. Marcovici-Mizrahi, H.E. Gottlieb, V. Marks, A. Nudelman, On the stabilization of the *syn* -rotamer of amino acid carbamate derivatives by hydrogen bonding, J. Org. Chem. 61 (1996) 8402–8406, https://doi.org/10.1021/jo961446u.
[44] C. Patrono, Cardiovascular effects of nonsteroidal anti-inflammatory drugs, Curr. Cardiol. Rep. 18 (2016) 25, https://doi.org/10.1007/s11886-016-0702-4.
[45] P. Khurana, S.M. Jachak, Chemistry and biology of microsomal prostaglandin E $_2$ synthase-1 (mPGES-1) inhibitors as novel anti-inflammatory agents: recent developments and current status, RSC Adv. 6 (2016) 28343–28369, https://doi.org/10.1039/C5RA25186A.
[46] A. Koeberle, H. Zettl, C. Greiner, M. Wurglics, M. Schubert-Zsilavecz, O. Werz, Pirinixic acid derivatives as novel dual inhibitors of microsomal prostaglandin E $_2$ synthase-1 and 5-lipoxygenase, J. Med. Chem. 51 (2008) 8068–8076, https://doi.org/10.1021/jm801085s.
[47] M. Murakami, H. Naraba, T. Tanioka, N. Semmyo, Y. Nakatani, F. Kojima, T. Ikeda, M. Fueki, A. Ueno, S. Oh-ishi, I. Kudo, Regulation of prostaglandin E2 biosynthesis by inducible membrane-associated prostaglandin E2 synthase that acts in concert with cyclooxygenase-2, J. Biol. Chem. 275 (2000) 32783–32792, https://doi.org/10.1074/jbc.M003505200.
[48] L. Zhang, Y. Li, M. Chen, X. Su, D. Yi, P. Lu, D. Zhu, 15-LO/15-HETE mediated vascular adventitia fibrosis via p38 MAPK-dependent TGF-β, J. Cell. Physiol. 229 (2014) 245–257, https://doi.org/10.1002/jcp.24443.
[49] Y. Wen, J. Gu, S.K. Chakrabarti, K. Aylor, J. Marshall, Y. Takahashi, T. Yoshimoto, J.L. Nadler, The role of 12/15-lipoxygenase in the expression of interleukin-6 and tumor necrosis factor-α in macrophages, Endocrinology 148 (2007) 1313–1322, https://doi.org/10.1210/en.2006-0665.
[50] Y.-J. Surh, K.-S. Chun, H.-H. Cha, S.S. Han, Y.-S. Keum, K.-K. Park, S.S. Lee, Molecular mechanisms underlying chemopreventive activities of anti-inflammatory phytochemicals: down-regulation of COX-2 and iNOS through suppression of NF-κB activation, Mutat. Res., Fundam. Mol. Mech. Mutagen. 480–481 (2001) 243–268, https://doi.org/10.1016/S0027-5107(01)00183-X.
[51] P. Banerjee, A.O. Eckert, A.K. Schrey, R. Preissner, ProTox-II: a webserver for the prediction of toxicity of chemicals, Nucleic Acids Res. 46 (2018) W257–W263, https://doi.org/10.1093/nar/gky318.
[52] A. Daina, O. Michielin, V. Zoete, SwissADME: a free web tool to evaluate pharmacokinetics, drug-likeness and medicinal chemistry friendliness of small molecules, Sci. Rep. 7 (2017) 42717, https://doi.org/10.1038/srep42717.
[53] D.F. Veber, S.R. Johnson, H.-Y. Cheng, B.R. Smith, K.W. Ward, K.D. Kopple, Molecular properties that influence the oral bioavailability of drug candidates, J. Med. Chem. 45 (2002) 2615–2623, https://doi.org/10.1021/jm020017n.
[54] A.L. Hopkins, C.R. Groom, A. Alex, Ligand efficiency: a useful metric for lead selection, Drug Discov. Today 9 (2004) 430–431, https://doi.org/10.1016/S1359-6446(04)03069-7.
[55] A.L. Hopkins, G.M. Keserü, P.D. Leeson, D.C. Rees, C.H. Reynolds, The role of ligand efficiency metrics in drug discovery, Nat. Rev. Drug Discov. 13 (2014) 105–121, https://doi.org/10.1038/nrd4163.
[56] Á. Tarcsay, K. Nyíri, G.M. Keserű, Impact of lipophilic efficiency on compound quality, J. Med. Chem. 55 (2012) 1252–1260, https://doi.org/10.1021/jm201388p.

[57] T.T. Wager, R.Y. Chandrasekaran, X. Hou, M.D. Troutman, P.R. Verhoest, A. Villalobos, Y. Will, Defining desirable central nervous system drug space through the alignment of molecular properties, in vitro ADME, and safety attributes, ACS Chem. Neurosci. 1 (2010) 420–434, https://doi.org/10.1021/cn100007x.

[58] H. Anh, N. Cuc, B. Tai, P. Yen, N. Nhiem, D. Thao, N. Nam, C. Van Minh, P. Van Kiem, Y. Kim, Synthesis of chromonylthiazolidines and their cytotoxicity to human cancer cell lines, Molecules 20 (2015) 1151–1160, https://doi.org/10.3390/molecules20011151.

[59] E.D. AlFadly, P.A. Elzahhar, A. Tramarin, S. Elkazaz, H. Shaltout, M.M. Abu-Serie, J. Janockova, O. Soukup, D.A. Ghareeb, A.F. El-Yazbi, R.W. Rafeh, N.-M.Z. Bakkar, F. Kobeissy, I. Iriepa, I. Moraleda, M.N.S. Saudi, M. Bartolini, A.S.F. Belal, Tackling neuroinflammation and cholinergic deficit in Alzheimer's disease: multi-target inhibitors of cholinesterases, cyclooxygenase-2 and 15-lipoxygenase, Eur. J. Med. Chem. 167 (2019) 161–186, https://doi.org/10.1016/j.ejmech.2019.02.012.

[60] P. Subramanium, S. Maran, Evaluation of anti-inflammatory and analgesic activities of methanolic leaf extract of the endangered tree species, Hildegardia populifolia (Roxb.) Schott and Endl, Int. J. Green Pharm. 9 (2015) 125, https://doi.org/10.4103/0973-8258.155062.

[61] A. Razmi, A. Zarghi, S. Arfaee, N. Naderi, M. Faizi, Evaluation of Anti-nociceptive and Anti-inflammatory Activities of Novel Chalcone Derivatives, 2013.

[62] S. Srivastava, C. Nath, M. Gupta, S. Vrat, J. Sinha, K. Dhawan, G. Gupta, Protection against gastric ulcer by verapamil, Pharmacol. Res. 23 (1991) 81–86, https://doi.org/10.1016/S1043-6618(05)80109-4.

[63] V. Lakshmi, V. Mishra, G. Palit, A new gastroprotective effect of limonoid compounds xyloccensins X and Y from xylocarpus molluccensis in rats, Nat Prod Bioprospect 4 (2014) 277–283, https://doi.org/10.1007/s13659-014-0034-2.

[64] Y.-H. Han, D.-Q. Chen, M.-H. Jin, Y.-H. Jin, J. Li, G.-N. Shen, W.-L. Li, Y.-X. Gong, Y.-Y. Mao, D.-P. Xie, D.-S. Lee, L.-Y. Yu, S.-U. Kim, J.-S. Kim, T. Kwon, Y.-D. Cui, H.-N. Sun, Anti-inflammatory effect of hispidin on LPS induced macrophage inflammation through MAPK and JAK1/STAT3 signaling pathways, Appl Biol Chem 63 (2020) 21, https://doi.org/10.1186/s13765-020-00504-2.

[65] P.A. Elzahhar, H.A. Nematalla, H. Al-Koussa, C. Abrahamian, A.F. El-Yazbi, L. Bodgi, J. Bou-Gharios, J. Azzi, J. Al Choboq, H.F. Labib, W.A. Kheir, M.M. Abu-Serie, M.A. Elrewiny, A.F. El-Yazbi, A.S.F. Belal, Inclusion of nitrofurantoin into the realm of cancer chemotherapy via biology-oriented synthesis and drug repurposing, J. Med. Chem. 66 (2023) 4565–4587, https://doi.org/10.1021/acs.jmedchem.2c01408.

[66] N.W. Hassan, A. Sabt, M.A.Z. El-Attar, M. Ora, A.E.-D.A. Bekhit, K. Amagase, A. A. Bekhit, A.S.F. Belal, P.A. Elzahhar, Modulating leishmanial pteridine metabolism machinery via some new coumarin-1,2,3-triazoles: design, synthesis and computational studies, Eur. J. Med. Chem. 253 (2023) 115333, https://doi.org/10.1016/j.ejmech.2023.115333.